

Issued: 5 October 1973

*CR 114675  
available to the Public*

FINAL REPORT

CR-114675

STUDY OF BLOOD FLOW SENSING

WITH MICROWAVE RADIOMETRY

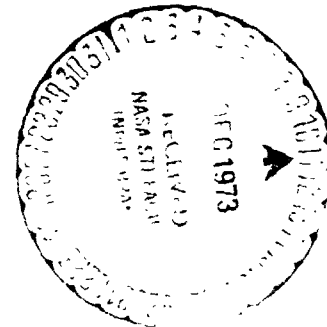
(NASA-CR-114675) STUDY OF BLOOD FLOW  
SENSING WITH MICROWAVE RADIOMETRY Final  
Report (Radiometric Technology, Inc.,  
Wakefield) 89 p HC \$6.50 CSCI 06P

#74-11889

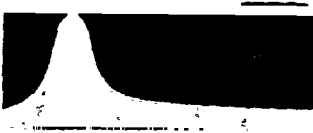
Unclas  
G3/04 23346

by Ronald A. Porter  
and Frank J. Wentz, III

CONTRACT NAS 2-7087



Prepared by



Radiometric Technology, Inc.  
280 VERNON STREET WAKEFIELD, MASSACHUSETTS

Prepared for

National Aeronautics and Space Administration

AMES RESEARCH CENTER

Moffett Field, California 94035

Issued: 5 October 1973

Final Report

STUDY OF BLOOD FLOW SENSING  
WITH MICROWAVE RADIOMETRY

by Ronald A. Porter  
and Frank J. Wentz, III

Contract NAS 2-7087

Distribution of this report is provided in the interest of information exchange. The responsibility for the contents resides with the authors or organization that prepared it.

Prepared by

RADIOMETRIC TECHNOLOGY, INC  
28C Vernon Street  
Wakefield, Massachusetts 01880

Prepared for

National Aeronautics and Space Administration  
AMES RESEARCH CENTER  
Moffett Field, California 94035

## ABSTRACT

A study and experimental investigation has been performed to determine the feasibility of measuring regional blood flow and volume in man by means of microwave radiometry. An indication was expected of regional blood flow from measurement of surface and subsurface temperatures with a sensitive radiometer.

Following theoretical modeling of biological tissue, to determine the optimum operating frequency for adequate sensing depth, a sensitive microwave radiometer was designed for operation at 793 MHz. A temperature sensitivity of 0.06°K rms was realized in this equipment.

Measurements performed on phantom tissue models, consisting of beef fat and lean beefsteak showed that the radiometer was capable of sensing temperatures from a depth between 3.8 and 5.1 cm.

Radiometric and thermodynamic temperature measurements were also performed on the hind thighs of large dogs. These showed that the radiometer could sense subsurface temperatures from a depth of, at least, 1.3 cm. Delays caused by externally-generated RF interference, coupled with the lack of reliable blood flow measurement equipment, prevented correlation of radiometer readings with regional blood flow. For the same reasons, it was not possible to extend the radiometric observations to human subjects.

A set of conclusions and recommendations are presented at the end of the report.

#### ACKNOWLEDGMENTS

The authors wish to acknowledge the valued assistance and cooperation of the following individuals in connection with this study:

Harry H. Miller, M.D.

New England Medical Center  
Hospitals, Boston, MA

William Carney, M.D.

New England Medical Center  
Hospitals, Boston, MA

## TABLE OF CONTENTS

	<u>Page</u>
SECTION 1 - INTRODUCTION -----	1-1
SECTION 2 - THEORETICAL STUDIES -----	2-1
2.1 Dielectric Permittivities of Biological Tissues -----	2-1
2.2 Brightness Temperature and Emissivity of Layered Media ----	2-9
2.3 Selection of Radiometer Operating Frequency -----	2-10
SECTION 3 - RADIOMETER DESIGN -----	3-1
3.1 Design Objectives -----	3-1
3.2 Basic Radiometer Configuration -----	3-1
3.3 Radiometer Design and Performance Characteristics -----	3-2
3.3.1 Radiometer Temperature Sensitivity -----	3-2
3.3.2 Other Design and Performance Characteristics -----	3-7
3.4 Radiometer Design Details -----	3-8
3.4.1 Dielectric-Loaded Waveguide Antenna -----	3-8
3.4.2 Radio Frequency Section -----	3-11
3.4.3 Calibration Section -----	3-15
3.4.4 Lock-In Amplifier -----	3-17
3.4.5 Radiometric Data System -----	3-17
3.5 Radiometer Calibration -----	3-25
3.6 Data Reduction -----	3-28
SECTION 4 - TEMPERATURE MEASUREMENTS ON DOGS -----	4-1
4.1 Measurements On First Dog -----	4-1
4.2 Measurements On Second Dog -----	4-4
4.3 Measurements On Third Dog -----	4-7
SECTION 5 - RADIOMETRIC OBSERVATIONS -----	5-1
5.1 Introduction -----	5-1
5.2 Phantom Measurements -----	5-1
5.3 Measurements On Large Dog -----	5-6
SECTION 6 - CONCLUSIONS -----	6-1

TABLE OF CONTENTS (Continued)

	<u>Page</u>
SECTION 7 - RECOMMENDATIONS -----	7-1
7.1 Integral VSWR Measurement Circuit -----	7-1
7.2 Measurement of Blood Distribution in the Body -----	7-1
7.3 Correlative Measurements of Blood Flow -----	7-2
7.4 Lower Frequency Radiometer -----	7-2
SECTION 8 - REFERENCES -----	8-1
APPENDIX A - LISTINGS OF COMPUTER PROGRAMS	

## LIST OF ILLUSTRATIONS

<u>Figure No.</u>		<u>Page</u>
2-1	Phantom Tissue Model -----	2-2
2-2	Dielectric Permittivity of Human Skin versus Frequency ---	2-4
2-3	Dielectric Permittivity of Human Fat versus Frequency ----	2-5
2-4	Dielectric Permittivity of Lean Beefsteak versus Frequency -	2-6
2-5	Dielectric Permittivity of Beef Bone versus Frequency ----	2-7
2-6	Brightness Temperature as a Function of Antenna Dielectric Constant -----	2-8
2-7	Brightness Temperature versus Frequency for a Model with Two Thicknesses of Muscle Tissue -----	2-11
2-8	Ratio of Change in Brightness Temperature to Change in Temperature versus Frequency, for Muscle Tissue Model ----	2-12
3-1	UHF Microwave Radiometer -----	3-3
3-2	Major Components in UHF Microwave Radiometer -----	3-4
3-3	Functional Block Diagram of UHF Radiometer -----	3-5
3-4	Dielectric-Loaded Waveguide Antenna -----	3-10
3-5	Functional Block Diagram of Radiometric Data System -----	3-19
3-6	Radiometer Calibration Data -----	3-27
3-7	Sample Computer Printout of Radiometric and Temperature Probe Data, for Final Dog Experiment -----	3-30
4-1	Dog's Leg Temperatures versus Time -----	4-2
4-2	Dog's Leg Temperatures versus Time -----	4-3
4-3	Radiometric Apparent Temperature versus Time -----	4-6
4-4	Electromagnetic Flowmeter Readings versus Time, Second Dog -	4-8
4-5	Temperatures versus Time, for Thigh of Third Dog -----	4-9
4-6	Temperatures versus Time, for Thigh of Third Dog -----	4-10
5-1	Phantom Model -----	5-2
5-2	Phantom Apparent Temperatures and Temperatures -----	5-3
5-3	Power Transmission versus Voltage Standing Wave Ratio ----	5-5
5-4	Apparent Temperature and Temperature Data on Dog's Thigh --	5-7
5-5	Apparent Temperature and Temperature Data on Dog's Thigh --	5-8

LIST OF TABLES

<u>Table No.</u>		<u>Page</u>
3-1	Radiometer Filter Characteristics -----	3-12
4-1	Temperature Drops in Test Leg -----	4-1
4-2	Temperature Changes in Reference and Test Legs -----	4-5



## Section 1

### INTRODUCTION

The purpose of the research described in this report was to conduct a study and experimental investigation aimed at determining the feasibility of measuring regional blood flow and volumes in man by means of microwave radiometric sensing techniques. Since microwave radiometers are temperature sensing instruments, it was expected that an indication of regional blood flow would be gained by measuring related temperatures down to a depth dictated by the selected operating frequency. The study has confirmed the ability of a sensitive radiometer to sense subsurface temperatures in living tissue, although the work schedule did not allow sufficient time for correlation of this information with regional blood flow.

The project involved the following basic elements of work:

- 1) A theoretical study to determine radiometric sensing depths of microwave thermal energy, emitted by models of biological tissue, over the frequency range 0.15 to 5 GHz. The purpose of this work was to locate an optimum operating frequency for the radiometer. This was established at 725 MHz.
- 2) Design and development of a sensitive microwave radiometer suitable for laboratory-type observations on tissue models, animals and human subjects. This was successfully accomplished; the radiometer operates at a frequency of 793 MHz and has a minimum detectable temperature sensitivity of 0.06 degree Kelvin rms, for a 10-second output time constant.
- 3) Radiometric and correlative temperature measurements on phantom models of biological tissue, consisting of beef fat and lean beefsteak, to determine the depth from which temperatures can be sensed. It was found that the radiometer sensed temperatures from a depth between 3.8 and 5.1 cm in lean beefsteak.
- 4) Temperature profile versus blood flow measurements on hind thighs of large dogs, without radiometric observations. Correlation of blood flow with surface and subsurface temperatures was accomplished with somewhat limited success due to problems encountered with the stability of electromagnetic flowmeters. Success was achieved only on a "go no-go" basis, in that measurements were made under full-flow or no-flow conditions - the no-flow condition was achieved through the use of

a tourniquet. Some temperature profiles were obtained after a given area was cooled with an ice-alcohol mixture.

5) Radiometric and correlative temperature observations on the hind thigh of a large dog. This investigation showed that the radiometer sensed temperatures from a depth of, at least, 1.3 cm.

The above work demonstrated clearly that radiometric measurement of subsurface temperature changes, associated with changes in blood flow, is feasible. Unfortunately, due to time limitations imposed by design changes, caused by externally generated RF interference, and the lack of adequate blood flow measuring equipment, it was not possible to establish a quantitative relationship between radiometer apparent temperatures and regional blood flow. The shortage of time also precluded any observations on human subjects.

Considering the problems encountered with externally-generated RF interference and the lack of reliable blood flow measurement equipment, it is felt that a good beginning has been made in the application of microwave radiometry to subsurface temperature sensing in living tissue. The results of the study are presented in the form of numerous plots, tables and related discussions.

A set of conclusions and recommendations are presented at the end of the report. It is felt that, if the recommendations are adopted and the requisite observations made on human subjects, the microwave radiometric technique can be properly developed and ultimately become quite useful for subsurface temperature sensing and indirect measurement of blood distribution in the human body.

## Section 2

### THEORETICAL STUDIES

Preliminary theoretical studies were conducted to determine the feasibility of using a radiometer to detect internal blood flow in living tissue. These studies also provided a method for selecting the optimum radiometer frequency for detecting blood flow. The tissue structure was modeled by a planar layered medium, of infinite lateral extent, because such a model allows for direct computations of brightness temperature. The temperature of the layer representing the region of internal blood flow was assumed to be indicative of the volume of blood flow. The optimum radiometer operating frequency for detecting changes in blood flow was determined by changing the temperature of this layer and finding the frequency at which the largest change in surface brightness temperature occurred.

#### 2.1 DIELECTRIC PERMITTIVITIES OF BIOLOGICAL TISSUES

The tissue structure was modeled by a planar layered medium of infinite lateral extent. The five media, shown in Figure 2-1, used for the model were, in descending order: the antenna, dielectric, skin, fat, muscle and bone. The antenna dielectric and bone layers were semi-infinite in thickness. The thickness of the skin layer was 0.3 cm, the fat layer was 0.5 cm, and the muscle layer thickness was a variable in the model. Before surface brightness temperatures could be computed, the dielectric permittivities of each layer needed to be specified.

Samples of lean beefsteak, representing muscle, beef bone, abdominal human fat, and human skin were submitted to the Laboratory for Insulation Research, at the Massachusetts Institute of Technology, for dielectric permittivity measurements at 0.5, 1 and 3 GHz. The beef bone appeared to be taken near a joint and contained little marrow. Measurements were made at two temperatures: 36°C and 40°C for the beefsteak, bone, and skin, and 27.5°C and 42.9°C for the fat. The permittivity of fat, at 36°C, was determined by a linear interpolation between 27.5°C and 42.9°C. Additional information was obtained from Pennock<sup>1</sup> on the permittivity of human skin, fat, and muscle at 0.15 GHz and at a temperature of 37°C. The measurements, made at

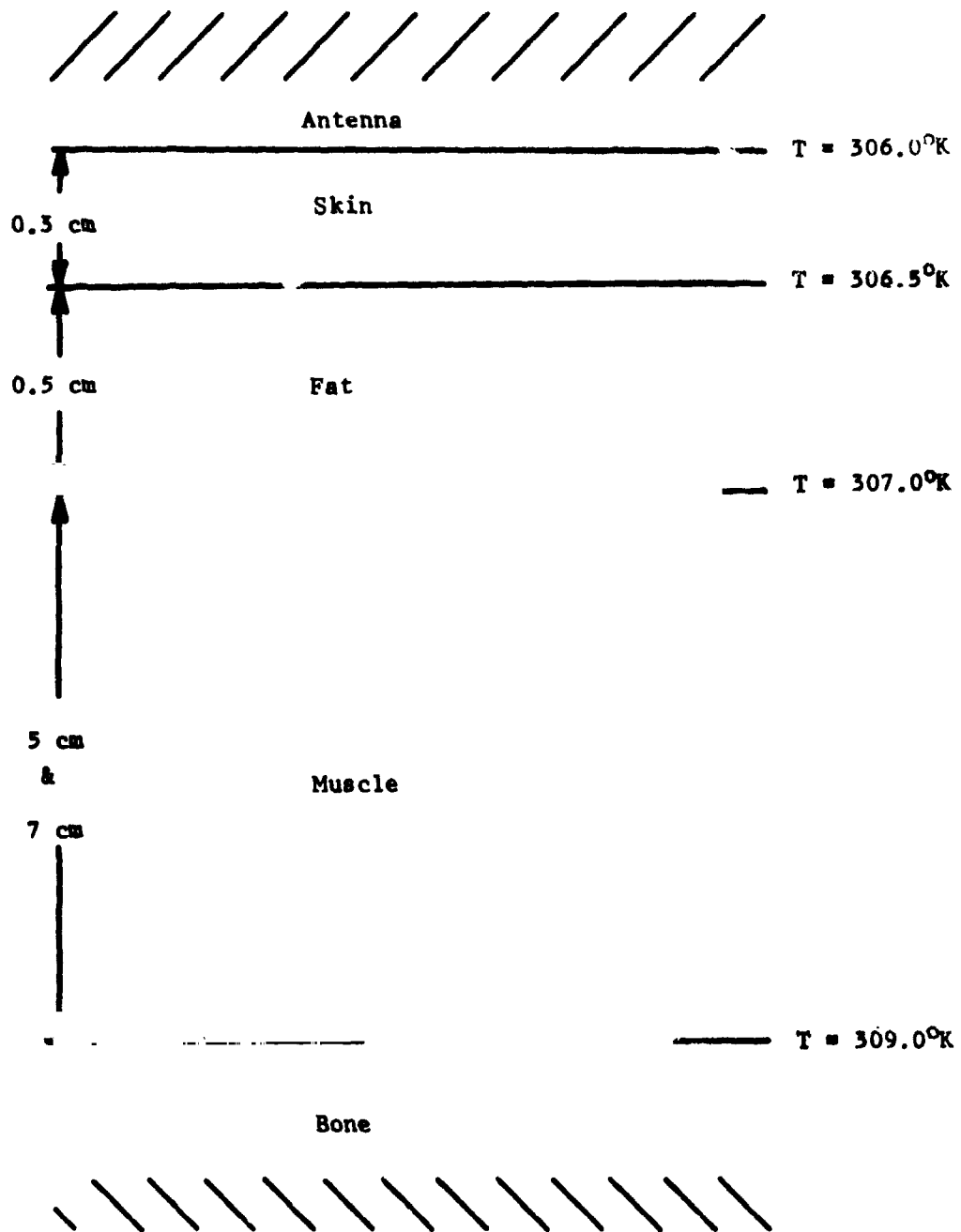


Figure 2-1 - Phantom Tissue Model

two temperatures, indicate that variations in permittivity with temperature is slight over a range of 1°C, and Pennock's data at 37°C should not be significantly different from measurements made at 36°C. The permittivity of bone at 0.15 GHz was determined by extrapolating the higher frequency data, noting that the variation of bone permittivity with frequency is slight.

Figures 2-2 through 2-5 show the complex permittivity,  $\epsilon' - j\epsilon''$ , as a function of frequency for a temperature of 36°C. By interpolating between the four data points, the permittivity at any frequency between 0.15 and 3 GHz can be approximated. The error in all measurements was about 5%. One factor which could contribute to the permittivity of dead tissue being different from living tissue is the absence of circulating fluids. Accordingly, great care was exercised in sealing tissue samples against evaporation.

The antenna dielectric was chosen to match, as close as possible, the tissue structure, while having negligible attenuation. To match the impedance of the model, consisting mainly of muscle tissue, in which the real part of the permittivity is high, the antenna should also have a large real permittivity. In order to exhibit negligible attenuation, the antenna imaginary permittivity should be as small as possible. The antenna chosen to meet these requirements has a permittivity of  $30 - j0.015$ . Further details on the antenna are given in Section 3.

A parametric study was conducted during the report period to assess the influence of the antenna dielectric constant on tissue brightness temperatures. The parameter involved in the study was fat thickness lying on top of muscle tissue.

Figure 2-6 shows the results of calculations performed, using Program LAYER, at 725 MHz. A muscle tissue thickness of 7 cm was used in the model. The plots show that, for a lean individual with a fat layer of 0.5 cm, the optimum dielectric constant is approximately 25. As the fat layer increases to 1.5 and 3.0 cm, the loading material should exhibit dielectric constants of 7 and 2.5, respectively. Since the peaks in the curves are fairly flat, considerable latitude should be acceptable in the value of the dielectric constant; this is estimated at  $\pm 40\%$ , for a brightness temperature error of 5°K.

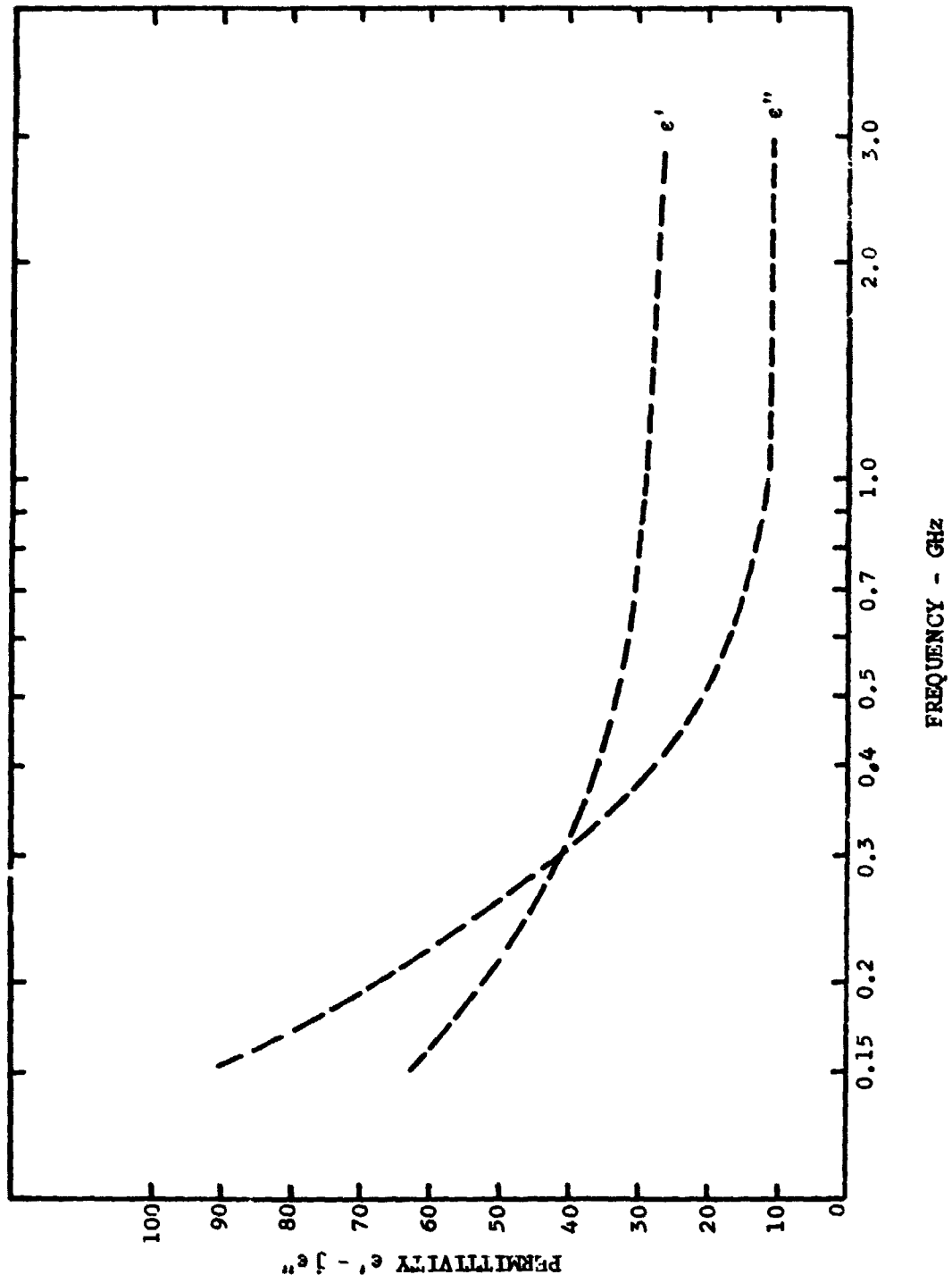


Figure 2-2 - Dielectric Permittivity of Human Skin versus Frequency

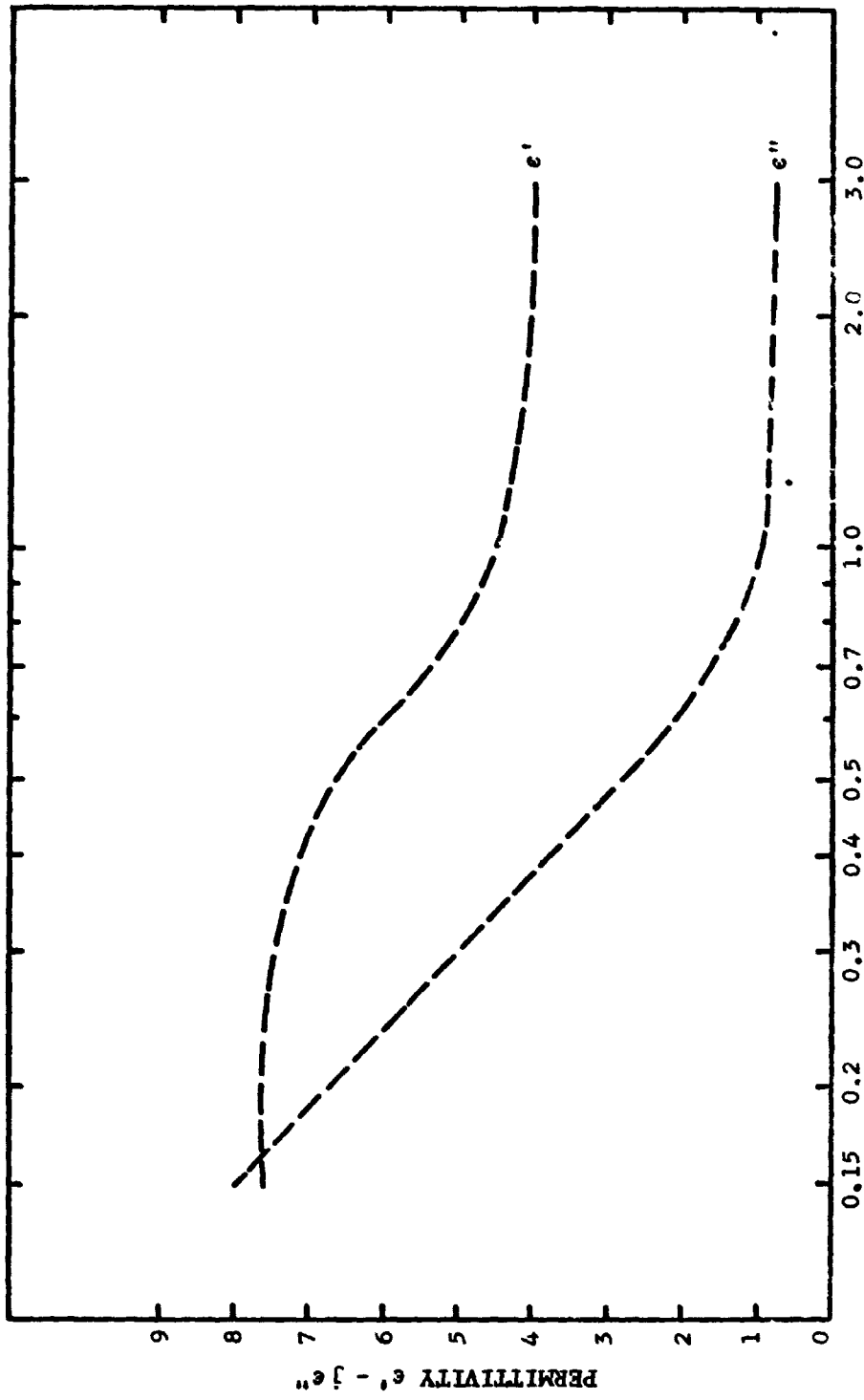


Figure 2-3 - Dielectric Permittivity of Human Fat versus Frequency

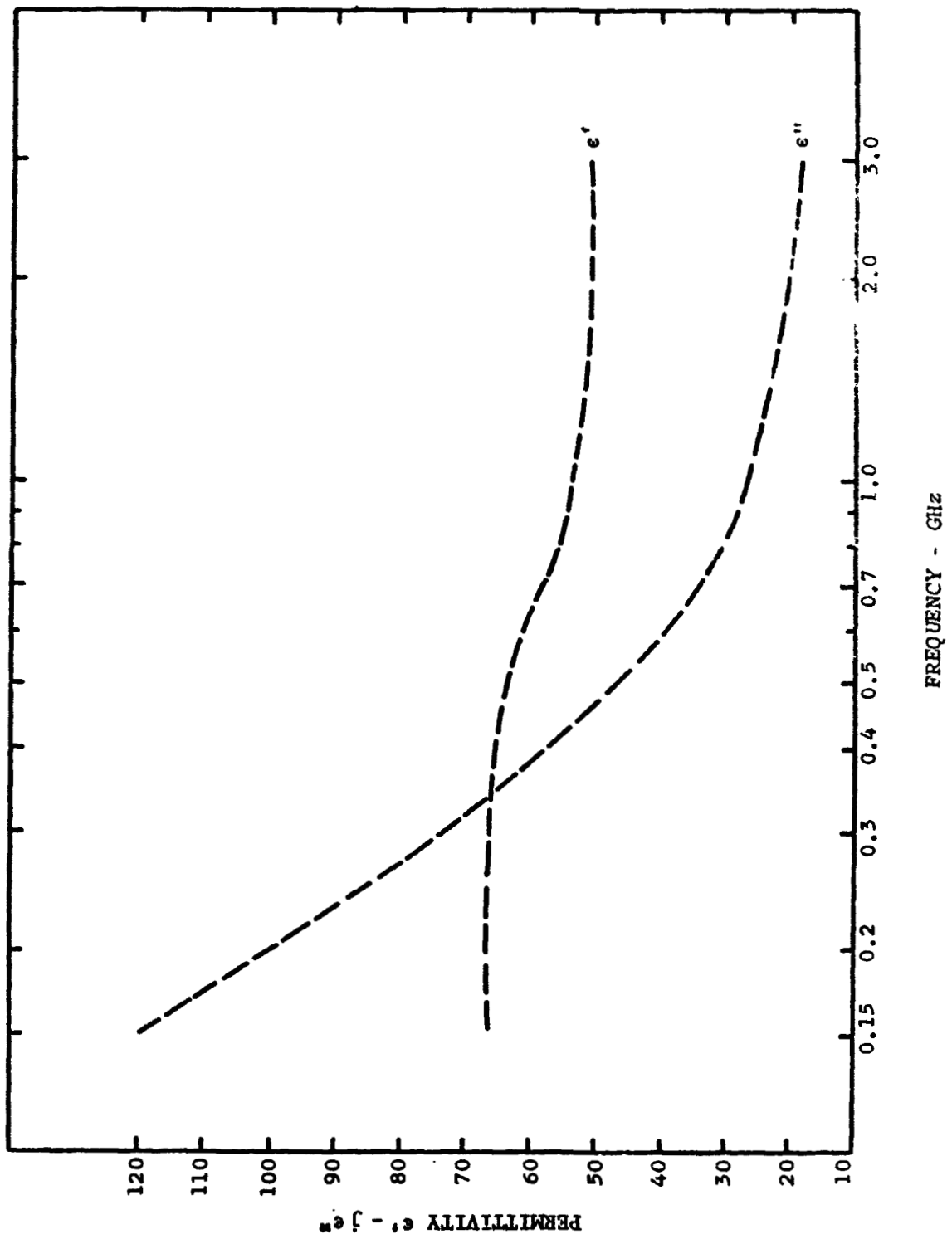


Figure 2-4 - Dielectric Permittivity of Lean Beefsteak versus Frequency



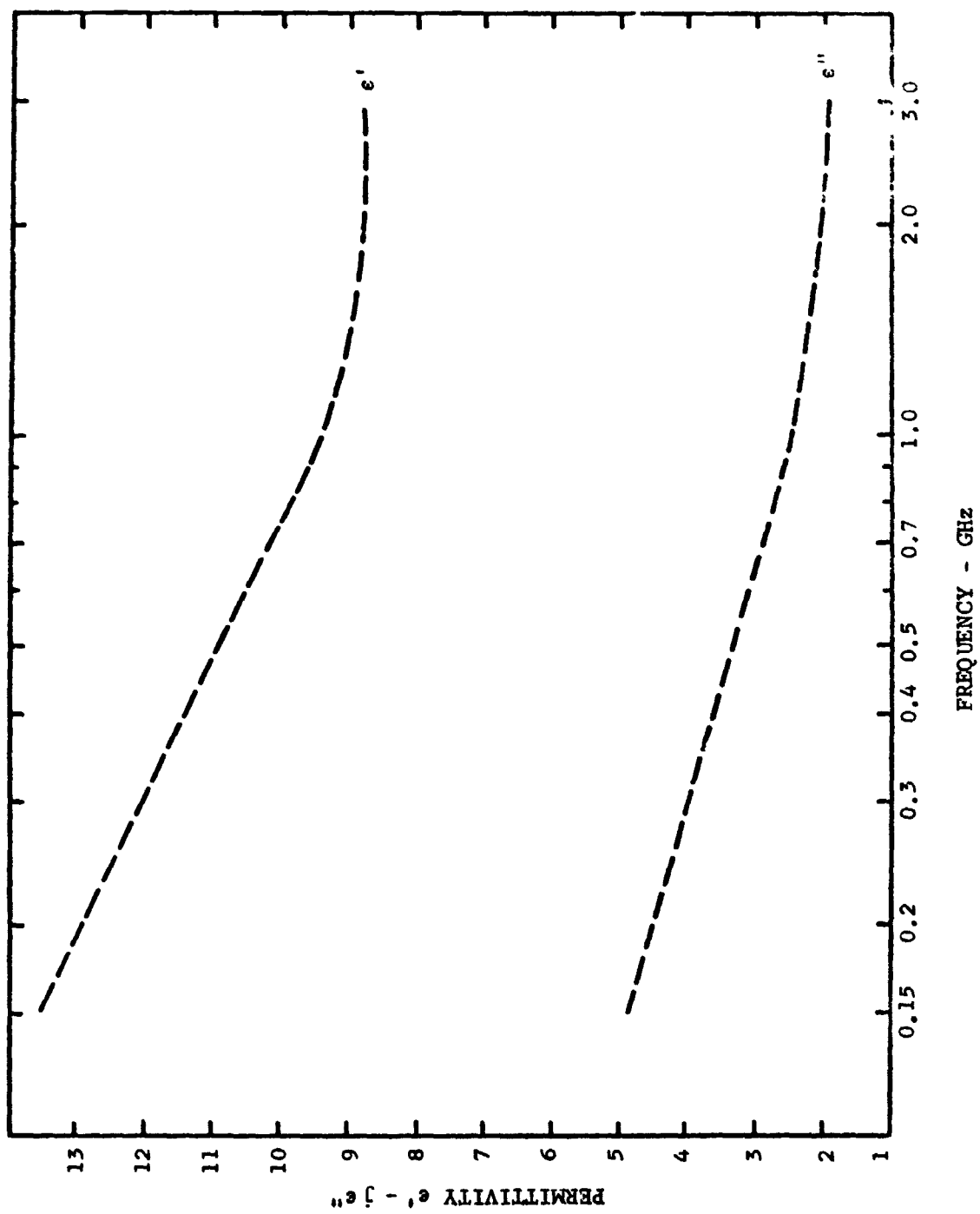


Figure 2-5 - Dielectric Permittivity of Beef Bone versus Frequency

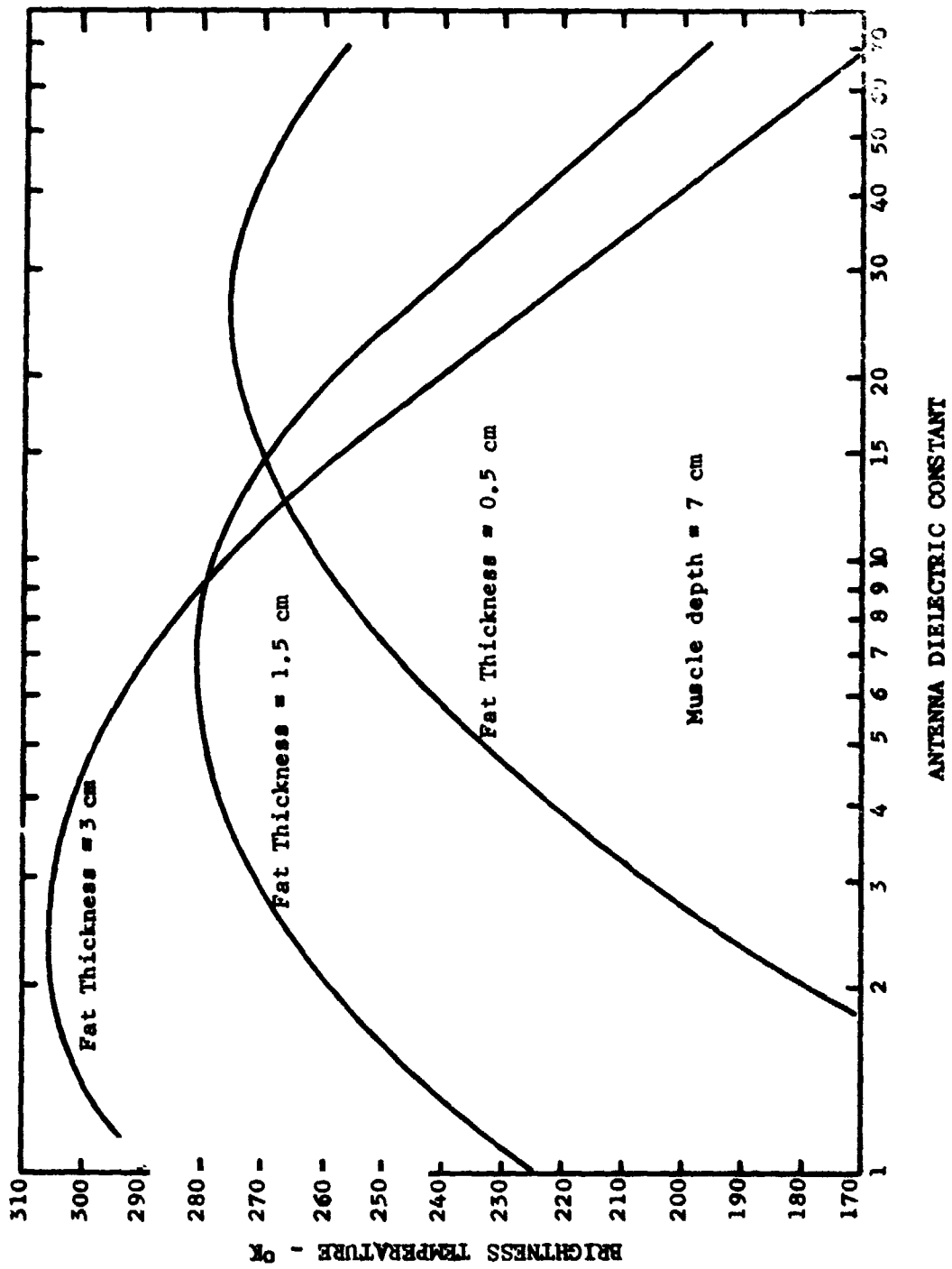


Figure 2-6 - Brightness Temperature as a Function of Antenna Dielectric Constant

As mentioned above, the antenna furnished for the radiometer is loaded with a material having a dielectric constant of 30. Based on the above criterion, this antenna should furnish adequate absolute brightness temperatures on all individuals exhibiting a fat layer of up to approximately 1.3 cm. This is expected to encompass a fairly large percentage of the male population.

## 2.2 BRIGHTNESS TEMPERATURE AND EMISSIVITY OF LAYERED MEDIA

The brightness temperature,  $T_B$ , referred to herein, is a measure of power being thermally radiated from the tissue layers upward into the antenna. The antenna also radiates power downward. A measure of this power is the internal radiometer temperature,  $T_R$ . A portion of  $T_R$  is reflected by the tissue layers back into the antenna. The apparent temperature,  $T_A$ , is a measure of the total power travelling upward into the antenna and is given by,

$$T_A = T_B + R T_R, \text{ } ^\circ\text{K} \quad (2-1)$$

where,  $R$  is the power reflectivity of the tissue layers.  $R$  is related to the emissivity  $\mathcal{E}$  of the tissue-antenna structure simply by,

$$R = 1 - \mathcal{E} \quad (2-2)$$

The emissivity  $\mathcal{E}$  can be found by assigning a constant temperature,  $T_0$ , to the layered medium, computing the brightness temperature,  $T_B$ , and then dividing  $T_B$  by  $T_0$ . That is,

$$\mathcal{E} = T_B / T_0 \quad (2-3)$$

Any  $T_0$  can be used because  $T_B$  is directly proportional to  $T_0$  i.e., the relationship between  $T_B$  and  $T_0$  is linear.

The brightness temperature of a layered medium depends on the permittivities, thicknesses, and temperatures of the various layers and on the radiation frequency and angle of incidence. With these inputs, a computer program LAYER (developed during previously conducted work under Company sponsorship) can compute  $T_B$ .

Computations at five frequencies (0.15, 0.5, 0.1725, 1.0, and 3.0 GHz) were performed for two muscle layer thicknesses of 5 and 7 cm. The temperatures of the layer interfaces were, in descending order, 306.0, 306.5, 307.0, 309.0°K, as shown in Figure 2-1. The temperature gradient within the layers was taken to be linear. Zero incidence angle was always used. Figure 2-7 shows the results of these computations. At the higher frequencies, radiation originating deep within the muscle layer and from the bone layer is, to a large degree, attenuated by the time it reaches the antenna. This explains the convergence of the curves for the 5 cm and 7 cm models at higher frequencies. The rise in brightness temperature, with increasing frequency, is due to a better impedance match between the antenna and the remaining layers at higher frequencies.

### 2.3 SELECTION OF RADIOMETER OPERATING FREQUENCY

In selecting the radiometer operating frequency, the temperature of the muscle layer was assumed to be indicative of the blood flow to be detected by the radiometer. By changing the muscle layer temperature and noting at which frequencies the largest change in brightness temperature occurs, the optimum radiometer frequency for sensing blood flow changes can be determined. Computations similar to those described in Section 2.2 were conducted in which the temperature of the muscle-bone interface was varied in increments of 0.2°K, from 307°K to 311°K. The brightness temperature,  $T_B$ , varies linearly with the temperature of the bottom interface. The change,  $\Delta T_B$ , in brightness temperature per change,  $\Delta T_0$ , in internal temperature of the bottom interface is plotted against frequency in Figure 2-8. A maximum is exhibited near 0.5 GHz, with the curves being fairly flat over the region of 0.15 to 1.0 GHz. The power attenuation through the various media varies directly with the imaginary part,  $\epsilon''$ , of the permittivity and with frequency. Figures 2-2 through 2-5 show that, at the lower frequencies,  $\epsilon''$  displays a sharp rise which causes the curves in Figure 2-8 to fall off with decreasing frequency. At the higher frequencies, where  $\epsilon''$  is fairly constant, the  $\Delta T_B/\Delta T_0$  curves also fall off because of the dependence of power attenuation on frequency.

Since the ratio,  $\Delta T_B/\Delta T_0$ , is a maximum at a frequency of 0.5 GHz, this would be an obvious choice of radiometer operating frequency. However, it was felt that

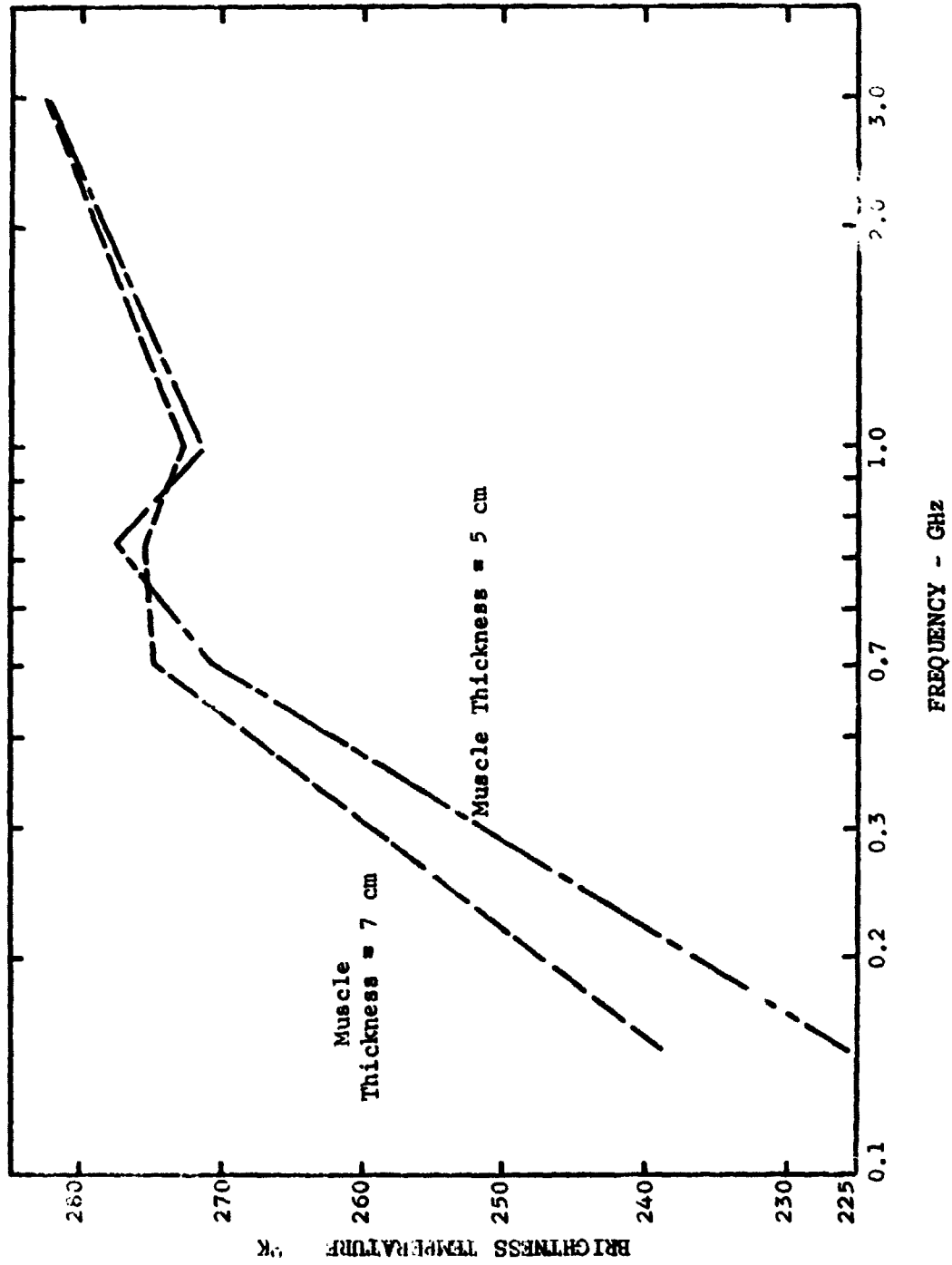


Figure 2.7 brightness Temperature versus Frequency for a Model with Two Thicknesses of Muscle Tissue

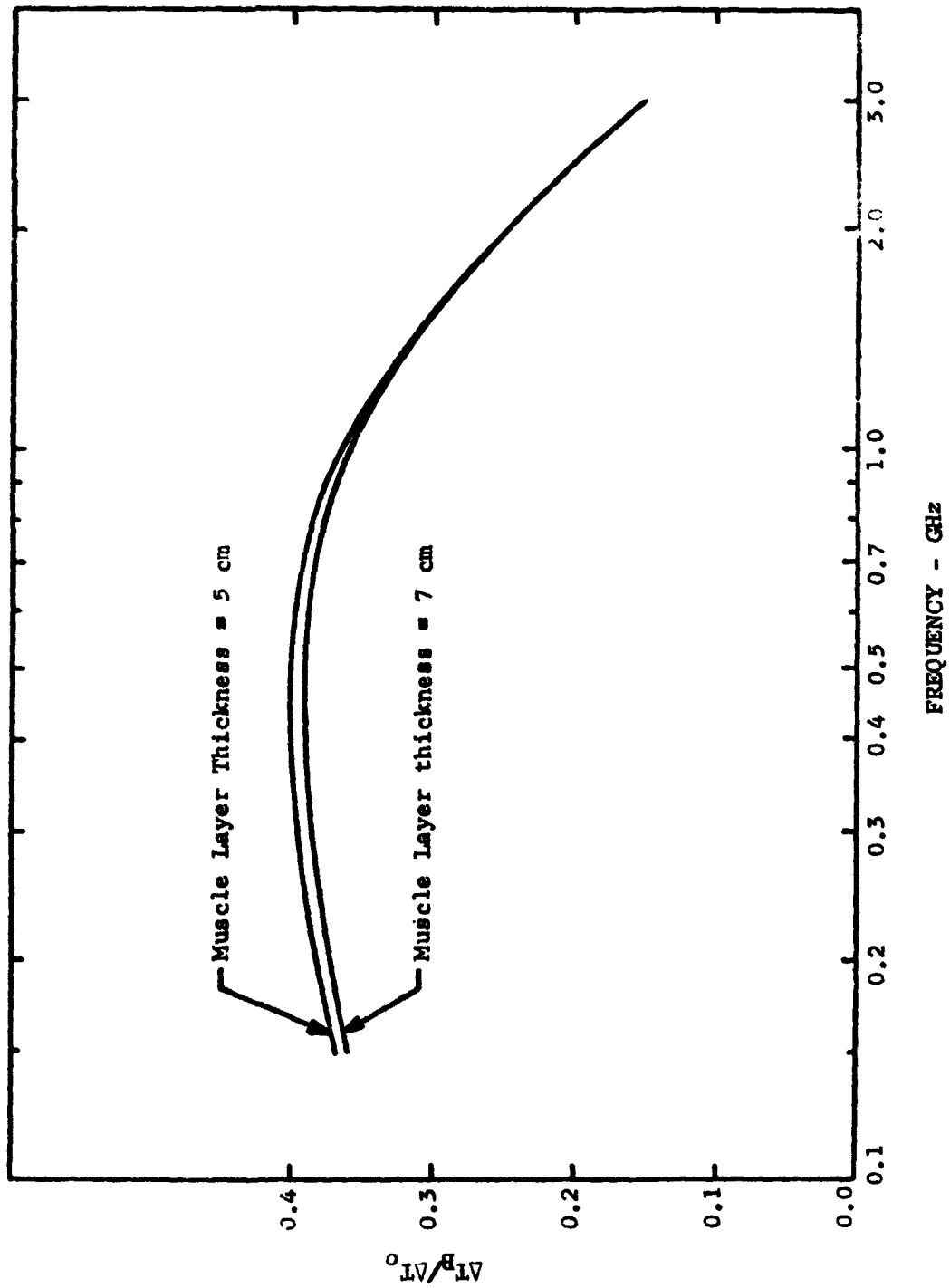


Figure 2-8 - Ratio of Change in Brightness Temperature to Change in Temperature versus Frequency, for Muscle Tissue Model

operation at such a low frequency would result in a rather large antenna aperture and, hence, poor spatial resolution. Accordingly, a search was conducted for a clear region higher in the UHF spectrum, referring to the Federal Communications Commission frequency allocations. The result of this work showed that the region between 650 and 800 MHz was clear, except for the Channel 56 UHF TV channel at 723 to 728 MHz. It was, therefore, decided to set the radiometer operating band in this frequency interval and provide a narrow-band rejection filter to eliminate any possible interference from this television channel.

## Section 3

### RADIOMETER DESIGN

#### 3.1 DESIGN OBJECTIVES

The design objectives for the microwave radiometer were as follows:

1. Operation at a fixed frequency, located somewhere in the range 0.5 to 5 GHz.
2. High temperature sensitivity - 0.06 degree Kelvin for a ten (10) second output time constant (or 0.2°K for a one (1) second time constant).
3. A manually controlled, movable RF head with a specially designed, small waveguide horn antenna, and
4. A portable console containing the low frequency (video) portion of the radiometer, and a signal processing and recording unit.

The above objectives have been realized with a relatively lightweight and portable system suitable for laboratory investigations of blood flow.

#### 3.2 BASIC RADIOMETER CONFIGURATION

The basic configuration of this equipment is that of a load-comparison Dicke<sup>2</sup> radiometer. This configuration greatly reduces spurious noise signals, caused by short-term receiver gain fluctuations, by shifting the post-detection signal spectrum up from DC to a carrier which is above the highest expected gain variation frequency. This is accomplished by modulating the RF signal, at a point between the antenna and receiver, and coherently detecting this signal after the second detector. It can be shown that changes in radiometer output voltage, due to short-term variations in receiver gain, are zero.

The modulating waveform is a 50%-duty-cycle square-wave; thus, the radiometer dwells 50% of the time on the antenna signal and 50% of the time on a resistive termination, commonly referred to as the reference load. This comparison between the input signal and reference load is performed by a diode-type switch.



Figure 3-1 shows a photograph of the radiometer. The individual components are shown labelled in Figure 3-2. A functional block diagram of the radiometric system is presented in Figure 3-3. Basically, the system consists of an antenna; internal calibration section; modulator switch (Dicke load-comparison switch); RF amplifier section; square-law detector/video amplifier unit; lock-in amplifier with coherent detector and low pass output filters; and a signal processing and recording unit. Further details, concerning these subdivisions, are presented in Paragraphs 3.3 and 3.4.

### 3.3 RADIOMETER DESIGN AND PERFORMANCE CHARACTERISTICS

The design and performance characteristics of the radiometer are presented in the paragraphs to follow in terms of minimum detectable temperature sensitivity and other important data.

#### 3.3.1 RADIOMETER TEMPERATURE SENSITIVITY

The minimum detectable temperature sensitivity of any radiometer is usually expressed in terms of a unit signal-to-noise power ratio at the output of the radiometer. This definition is based upon a number of parameters whose actual values are referred to the input of the radiometer. These parameters include the input losses, input noise figure, and the effective passband of the radiometer.

The minimum detectable temperature sensitivity,  $\Delta T$ , is usually expressed as follows:

$$\Delta T = \frac{k \left[ (FL-1) T_o + T_a \right]}{\sqrt{B\tau}}, \text{ } ^\circ\text{K rms} \quad (3-1)$$

where,

$k$  is a constant depending on the character of the waveform employed for input signal commutation; this is usually set at a value of 2 for square-wave input chopping.

$(FL-1)$  represents the effective receiver noise figure.

REPRODUCIBILITY OF THE ORIGINAL PAGE IS POOR.

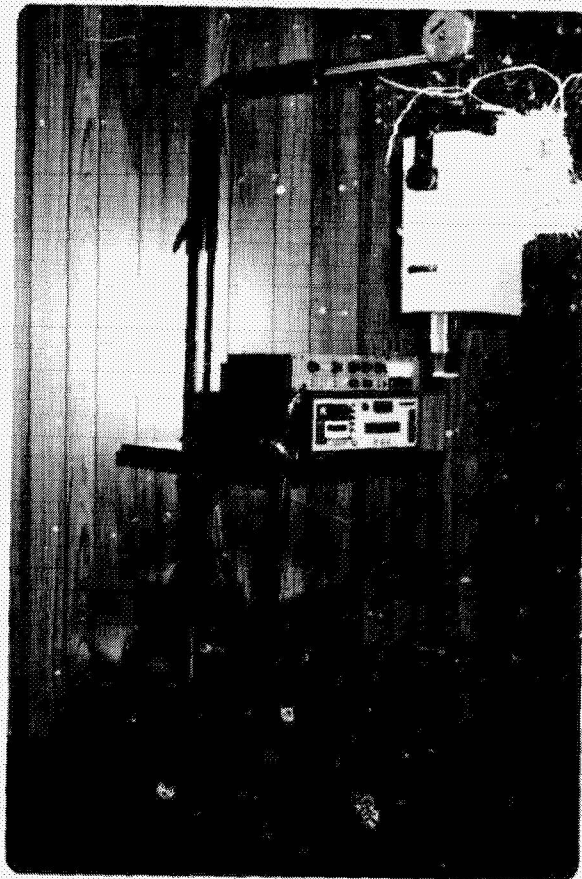


Figure 3-1 UHF Microwave Radiometer

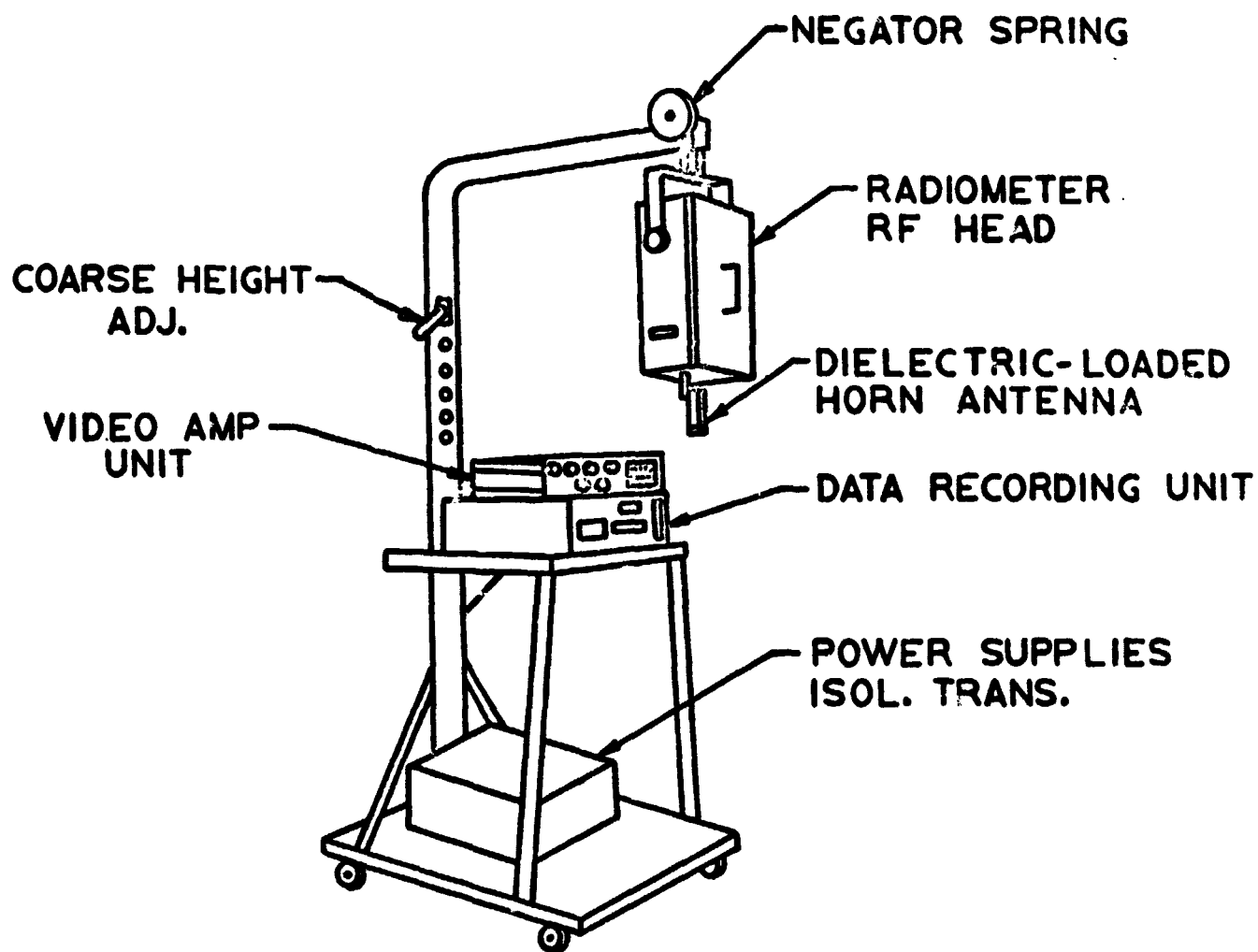


Figure 3-2 - Major Components in UHF Microwave Radiometer

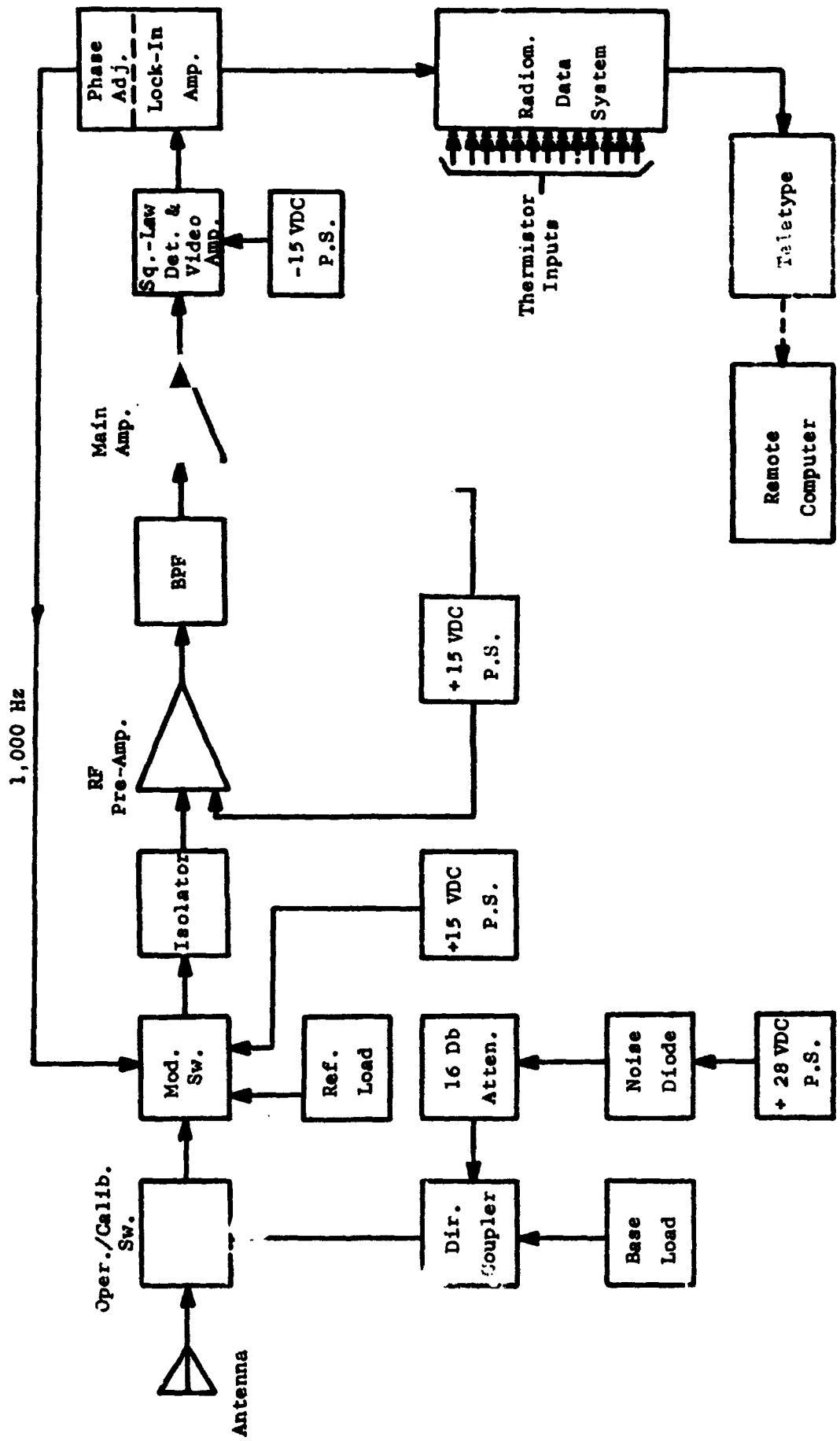


Figure 3-3 - Functional Block Diagram of UHF Radiometer

- F is the noise figure of the first detector (in this particular radiometer it is the first RF amplifier).
- L represents the sum of all the input losses, between the mouth of the antenna and the first RF amplifier.
- T<sub>o</sub> is the ambient radiometer RF head temperature (°K).
- T<sub>a</sub> is the average apparent temperature seen by the antenna (°K).
- B is the 3-db RF bandwidth prior to detection (Hz).
- τ is the radiometer output time constant (seconds).

In this design, the above parameters are as follows:

- k = 2
- F = 2.4 db (numerical value = 1.74)
- L = 2.2 db (numerical value = 1.66)
- T<sub>o</sub> = 311°K
- T<sub>a</sub> = 200°K
- B = 75 MHz at NASA-Ames. B = 119 MHz at Radiometric Technology, Inc.

From the above values it is possible to calculate the temperature sensitivity, ΔT, for an output time constant of one (1) second:

$$\Delta T = \frac{2[(1.74 \times 1.66 - 1) 311 + 200]}{\sqrt{75 \times 10^6 \times 1}} = 0.18^\circ\text{K rms}$$

For a 10-second time constant, the temperature sensitivity would improve by a factor of  $\sqrt{10}$ , or 3.16. Thus, for this time constant,  $\Delta T = \frac{0.19}{3.16} = 0.06^\circ\text{K rms}$ .

These sensitivities meet the original objective of 0.2°K and 0.06°K, for time constants of 1 and 10 seconds, respectively.

### 3.3.2 OTHER DESIGN AND PERFORMANCE CHARACTERISTICS

The other important radiometer performance characteristics are summarized below:

Operating RF center frequency	793 MHz at NASA-Ames 735 MHz at Radiometric Technology, Inc.
Antenna type	Dielectric-loaded waveguide horn antenna.
Dielectric constant of antenna loading material	30-j0.015 (Emerson & Cummings, Inc. stycast).
Antenna over-all dimensions	2.220 × 1.142 in.
Antenna inside dimensions	2.156 × 1.078 in.
Teflon antenna boot	1/32 in. teflon, dielectric constant = 2.1 - j0.017.
Antenna and input losses	2.2 db total.
Type of RF amplifier	Low noise transistor amplifier, operating at ambient temperature. First amplifier noise figure = 2.4 db.
RF amplifier gain (2 amplifiers)	23 + 43 = 66 db.
RF 3-db bandwidth	75 MHz at NASA-Ames; 119 MHz at Radiometric Technology, Inc. RF bandwidth defined by bandpass filter.
Modulator switch switching wave	1,000 Hz 50%-duty-cycle square wave.
Output detector/amplifier	Square-law characteristic in detector. Video amplifier integral with detector. Amplifier gain = 20 db.
Input calibration method	2-point calibration, at 0 and 53°K, using noise diode source.
RF head temperature	Stabilized at 311 ± 0.5°K after 45-minute warm-up.
Output time constants	0.1, 0.3, 1, 3, 10 & 30 secs., and external connection. Also, 1, 3, 10 & 30 usecs. and external connection. These are available in the Lock-In Amplifier unit.

Radiometer temperature sensitivity	0.18°K rms, for 1 sec., time constant 0.06°K rms, for 10 sec., time constant.
Radiometer absolute accuracy	± 0.5°K, at or near a null at the input.
Signal processing and recording method	Analog-to-digital conversion of radiometer and temperature probe inputs. Recorded on 2-track incremental digital magnetic tape cassette recorder.
Radiometer input power	115 VAC, 60 Hz, 2.5 amps.. Including heater.
Auxiliary instrumentation	Antenna calibration box. Thermistor temperature probes: Surface temperature Needle-type temperature probes Rectal temperature Air temperature.

### 3.4 RADIOMETER DESIGN DETAILS

The design aspects of the various subdivisions of the radiometer will be discussed with reference to Figure 3-3, which shows the functional block diagram of the system.

#### 3.4.1 DIELECTRIC-LOADED WAVEGUIDE ANTENNA

A factor that affects the transfer of power from the human body to an open waveguide antenna, connected to a radiometer, is the rather large disparity between the characteristic impedance of the body and that of free space. If one were to use a horn which is designed to produce efficient transfer of power from free space into a waveguide, as a means for transferring power from the human body to the waveguide, one would be confronted with a somewhat large impedance mismatch.

The characteristic impedance  $Z_{00}$  of free space is equal to  $\sqrt{\frac{\mu_0}{\epsilon_0}} = 377$  ohms.

The characteristic impedance  $Z_0$  of muscle tissue, at 800 MHz can be determined from the fact that its dielectric constant,  $K$ , is approximately  $58 - j38$ . Substituting

this value of K into the formula for the characteristic impedance, it is found that it is approximately one-seventh that of free space and that, because of the finite conductivity, this impedance is not quite real. A more important factor is that the impedance,  $Z_0$ , of the body is relatively low compared with that of free space.

If one were to design a horn, for transfer of power from a waveguide into free space, and vice versa, and fill it with a material having a dielectric constant of approximately 58 and, at the same time, decrease the dimensions of the horn by the factor  $\sqrt{58}$ , the horn would transfer power efficiently into a medium with a dielectric constant of 58.

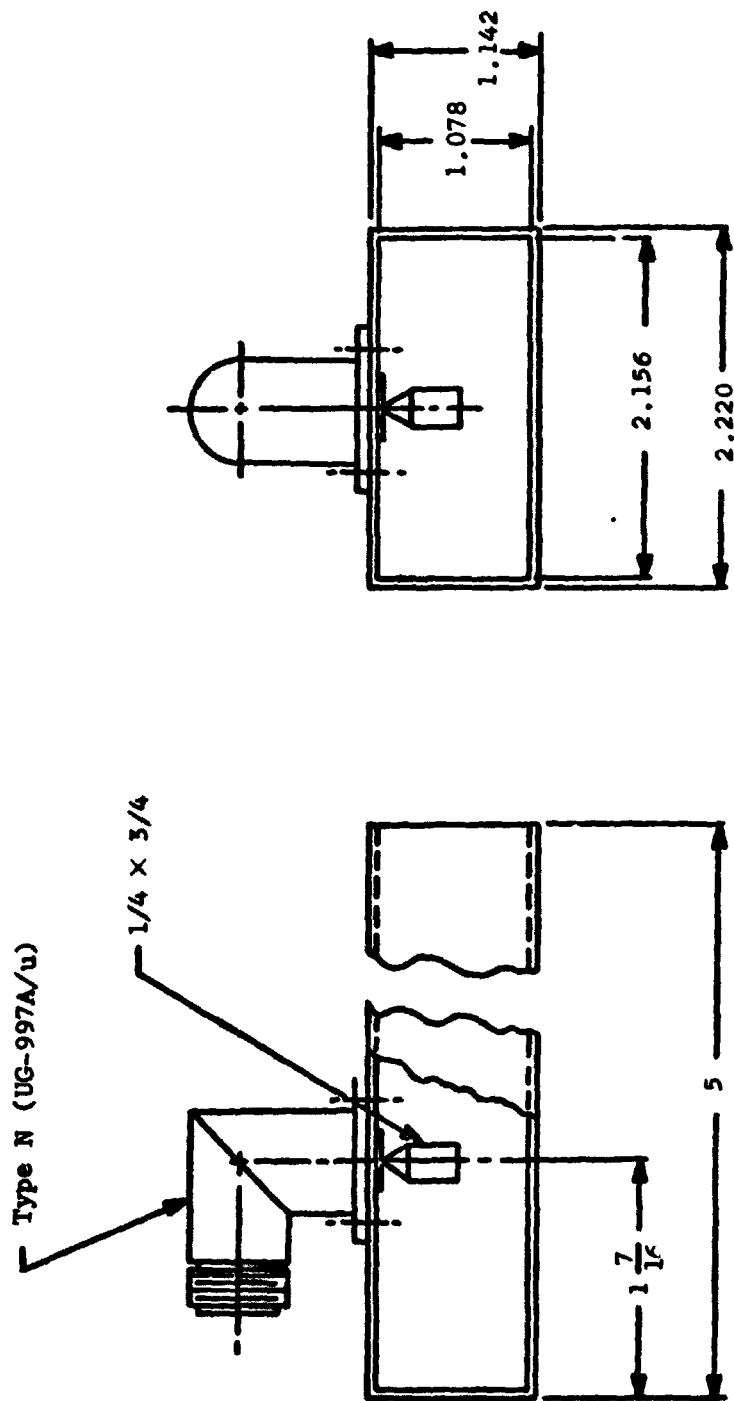
The dimensions of the waveguide horn would shrink by a factor of about seven. Such a horn can be fed with a coaxial line. Since the characteristic impedance of the waveguide, filled with a dielectric  $K = 58$ , would be about one-seventh of the conventional waveguide, the interface mismatch between the 50-ohm coaxial line and this device would be less than it is usually; thus the device for coupling a coaxial line to this type of an antenna does not present a design problem.

The antenna designed for the radiometer reflects the above approach. Figure 3-4 shows two views of the antenna. It will be noted that the dielectric material, used for loading the antenna, has a dielectric constant of 30 instead of 58. The reason for this is that the supplier no longer has any materials with dielectric constants greater than 30. This has not created any serious problem since the exact value is not very critical. Voltage-standing-wave-ratio (VSWR) measurements, performed on beef samples and the calves of several human legs gave readings of 1.5:1 to 2.4:1, depending on the thickness of the intervening fat layer.

Since the radiometer is a broad band device, the antenna bandwidth was made slightly wider than that occupied by the radiometer. This was accomplished by proper positioning of the end plate on the antenna and length of coupling probe.

Due to the very low loss tangent (0.0005) of the dielectric loading material, the power loss through the antenna is almost negligible.





Material:

Waveguide --- Brass

Dielectric --- Stycast K' = 30

Emerson & Cummings Inc.

Figure 3-4 - Dielectric-Loaded Waveguide Antenna

### 3.4.2 RADIO FREQUENCY SECTION

The RF section of the radiometer consists of two parts:

1. The RF amplifier section lying between the Calibration Switch and Square-Law Detector, and
2. The radiometer Calibration Section.

All of the RF components have 50-ohm input and output impedances and are interconnected with miniature semi-rigid 50-ohm coaxial cable. In many cases, interconnections are accomplished directly with miniature SMA-type connectors satisfying the requirements of MIL-C-39012.

#### 1. RF Amplifier Section

Referring to Figure 3-3, after the signal from the antenna passes through the Calibration Switch, it is applied to the microwave diode Modulator Switch. This component is operated at a 1,000 Hz rate by a 50%-duty-cycle square wave generated by an oscillator in the Lock-In Amplifier. Thus, the switch dwells one-half the time on the signal and the other half of the time on a resistive termination, commonly referred to as the Reference Load.

A Phase Adjustment circuit in the Lock-In Amplifier permits correct phasing of the 1,000 Hz square wave at the Modulator Switch so that its operation is synchronized with that of the coherent detector in the Lock-In Amplifier.

The switch has an insertion loss of 0.7 db, a VSWR of 1.35:1 and isolation, between terminals, of 70 db.

An isolator is located between the Modulator Switch and the low-noise RF Pre-Amplifier to provide isolation, for the pre-amplifier, from impedance fluctuations at the output of the Modulator Switch. The isolator provides 23 db isolation and has a forward insertion loss of 0.3 db.

The RF portion of the radiometer is, basically, a sensitive fixed-tuned radio frequency (TRF) receiver. It was not necessary to resort to a superheterodyne configuration, in this design, due to the availability of low-noise solid state RF amplifiers.

RF signal amplification and bandpass shaping is provided by two low-noise transistor amplifiers and a bandpass filter. The first amplifier has a noise figure of 2.4 db and gain of 23 db. In the absence of the bandpass filter, the amplifiers exhibit a rather broad 3-db bandwidth, from 590 to 830 MHz (240 MHz). Although a broad operating bandwidth is desirable in a radiometer, for reasons of improved temperature sensitivity, the lower end of this bandpass overlaps the UHF television broadcasting band. Thus, to eliminate TV interference, a steep-sided bandpass filter was added to the amplifier section. The filter 3-db bandpass extends from 755 to 904 MHz (150 MHz); however, since the upper frequency cutoff, in the RF amplifiers, is at 830 MHz the net passband is 75 MHz (755 - 830 MHz). The bandpass filter provides 61 db rejection at 716 MHz (Channel 54) which is the highest UHF TV frequency in the NASA-Ames area. Tests at NASA-Ames have shown this amount of rejection to be adequate for proper operation of the radiometer. The insertion loss of the filter is 0.8 db, from 760 to 901 MHz.

It should be mentioned that, at the Radiometric Technology, Inc., facility a different bandpass filter and a band rejection filter were required to eliminate UHF TV interference. The bandpass filter allowed a 3-db bandwidth of 119 MHz, in the radiometer after rejection of Channel 56 with an interdigital-type band rejection filter. The characteristics of all three filters are given in Table 3-1.

Table 3-1

RADIOMETER FILTER CHARACTERISTICS

Filter Type	3-db Bandpass (MHz)	Stop Band Rejection	Insertion Loss	VSWR
Bandpass (At NASA-Ames)	755 - 904	61 db @ 716 MHz* 60 db @ 936 MHz	0.8 db from 760 to 901 MHz	1.5 : 1
Bandpass (At Radiometric Tech., Inc.)	700 - 890	52 db @ 660 MHz >70 db @ 625 MHz	0.8 db from 720 to 805 MHz	1.5 : 1
Band Rejection (At Radiometric Technology, Inc.)	--	3 db from 720 to 730 MHz. 60 db from 723 to 728 MHz.	--	1.5 : 1

\*Highest interfering UHF TV frequency.

It should be mentioned that, although UHF TV interference has been eliminated through the use of the above filters, some interference is caused by fluorescent lights. This is only present when the radiometer is being used in the normal Operate mode and amounts to approximately 12°K at the output of the radiometer.

Since this interference is relatively broad band and cannot be eliminated by filtering, the radiometer should be operated only in areas where incandescent lighting is available. Wherever possible, nearby fluorescent lights, in adjoining rooms, should be switched off.

The second RF amplifier has a gain of 43 db and a noise figure of 4.1 db in the passband used at NASA-Ames. The total RF gain, represented by the two RF amplifiers and the intervening bandpass filter, is 65 db. The signal level at the input to the Square-Law Detector/Video Amplifier unit may be determined by calculating the noise temperature of the receiver and, then, substituting the result in the equation,

$$P_N = kTB \quad (3-2)$$

where,

$P_N$  = equivalent noise power

$k$  = Boltzmann's constant

and  $B$  = receiver bandwidth

The noise temperature of the RF amplifier section, referred to the input terminals of the first amplifier, may be calculated with the aid of the expression,

$$NT = (F - 1) T \quad (3-3)$$

where,

$NT$  is the noise temperature, °K

$F$  is the amplifier noise figure

and  $T$  is the ambient temperature of the amplifier, °K.

Now  $F = 2.4$  db (1.74 numerical value)  
and  $T = 311^{\circ}\text{K}$

Therefore,  $NT = (1.74 - 1) 311 = 230^{\circ}\text{K}$

Now,  $k = 1.38 \times 10^{-23}$   
and  $B = 75 \times 10^6$

Thus, the equivalent noise power at the input to the first RF amplifier, is

$$P_N = 1.38 \times 10^{-23} \times 230 \times 75 \times 10^6$$
$$= 2.38 \times 10^{-13} \text{ watts}$$

or  $P_N = 2,380 \times 10^{-13}$  milliwatts

Converting to dbm, where  $\text{db} = 10 \log \frac{P_1}{P_2}$ ,

$$P_N = 10(-13) + 10 \log 2,380$$
$$= -130 + (10 \times 3.376)$$

or  $P_N = -96$  dbm.

With a total gain of 65 db in the amplifier section, the signal level at the input to the Square-Law Detector is -31 dbm.

## 2. Square-Law Detector/Video Amplifier

The function of the Square-Law Detector/Video Amplifier unit is to recover the low frequency components of the radiometer input signal and provide output voltages that are proportional to input power. The tangential signal sensitivity of the unit is -51 dbm. Thus, the -31 dbm signal level, calculated in the preceding paragraph, is adequate for proper operation of the detector. This input level does not overload the detector/amplifier unit. Other characteristics of this unit are as follows:

RF frequency band: 600 - 800 MHz

Video Bandwidth: > 100 KHz

VSWR: 1.7 : 1

### 3.4.3 CALIBRATION SECTION

The purpose of this portion of the radiometer is to provide a means of establishing a zero baseline for all signal levels and to furnish a noise temperature calibration signal, of known amplitude, so that output voltages may be accurately converted to noise temperature, at the input to the radiometer, at any point in a given time interval.

As shown in Figure 3-3, the Calibration Section consists, in part, of a resistive termination (Base Load) connected to the input of the Modulator Switch via a directional coupler and the Operate/Calibrate coaxial switch. When the switch is in the Calibrate position, and the Noise Source is switched off, the Modulator switch is operating between two resistive terminations at essentially the same temperature - the Base Load and Reference Load - and the radiometer input is at a null. This establishes the zero baseline for all signal and calibration levels at the input of the radiometer.

When the noise diode is switched on, it generates a noise temperature, in excess of the standard ambient temperature (290 degrees Kelvin) by a specified number of decibels. Thus,

$$\text{Excess noise temp.} = \text{db excess noise (numerical)} \times 290, \text{ } ^\circ\text{K} \quad (3-4)$$

In this particular radiometer, the excess noise capability of the noise diode is 26.65 db, at a frequency of 800 MHz. This corresponds to a numerical value of 462.4. Thus, in this case,

$$\text{Excess noise temp.} = 462.4 \times 290 = 134,096^\circ\text{K}$$

To determine the noise temperature at the input to the Modulator switch, it is necessary to take into account signal attenuation, by the intervening lossy components, and re-radiation by the components at their ambient temperature. This is accomplished through the use of the well-known expression,

$$T_{\text{No}} = \frac{T_{\text{Ni}}}{L} + T \left(1 - \frac{1}{L}\right), \text{ } ^\circ\text{K} \quad (3-5)$$

or, 
$$T_{No} = T + (T_{Ni} - T) \frac{1}{L}, \text{ } ^\circ\text{K} \quad (3-6)$$

where,

$T_{No}$  is the noise temperature at the output of the lossy component

$T_{Ni}$  is the noise temperature at the input of the lossy component

$T$  is the thermodynamic temperature of the component

and  $L$  is the attenuating loss through the component.

The lossy components consist of the fixed attenuator, interconnecting coaxial cables and the Operate/Calibrate coaxial switch. The directional coupler involves a  $20 \pm 1$  db coupling loss, with negligible insertion loss. Listed below are the attenuation values of the lossy components:

Fixed attenuator	$16 \pm 0.5$ db
Interconnections and coaxial switch	0.3 db (estimate)

Using Equation (3-5) iterative calculations were performed to determine the output noise temperatures of the above components, allowing a 20-db nominal coupling loss between them. The result is a noise temperature of  $55^\circ\text{K}$  at the input to the Modulator Switch. As discussed in Section 3.5, the value derived from over-all radiometer calibration, using a standard hot-cold noise generator, was  $53.1^\circ\text{K}$ . The agreement is rather close between the calculated and derived values. This indicates that the error involved in using nominal losses for the attenuator and directional coupler, and an estimate for the remaining losses, was fairly small.

The above method of generating an internal calibration signal is simple and reliable, particularly if the ambient temperature of the components is held within close limits over the periods of time involved in radiometric measurements. As stated in Section 3.3.2, the RF head temperature was stabilized at  $311 \pm 0.5^\circ\text{K}$  during measurements performed with the radiometer.

It is worth observing that good long-term stability and absolute accuracy are dependent on close control of RF head temperature. The above uncertainty of

$\pm 0.5^{\circ}\text{K}$  can be largely reduced through the use of a proportional temperature controller with finer resolution and the application of a thicker layer of insulation on the inner walls of the RF head. Calibration signal stability can also be improved by keeping the DC power on the noise diode continuously and placing an on-off switch between the fixed attenuator and directional coupler.

#### 3.4.4 LOCK-IN AMPLIFIER

The Lock-In Amplifier is a standard fixed frequency commercial unit furnished by Princeton Applied Research Corporation. Their Model 120 is used in the radiometric system.

Lock-in amplifiers are used widely in radiometry due to their ability to measure very small changes in amplitude in slowly varying AC signals, which are usually obscured by high amplitude noise. In Equation (3-1) the noise temperature of a radiometer is expressed by the term  $(F-1)T_0$ . The value of this term is  $588^{\circ}\text{K}$  in this radiometer. With a 10-second output time constant, the radiometer is capable of measuring changes of  $0.06^{\circ}\text{K}$ . This represents 0.01% of the noise temperature of the radiometer. Clearly, the lock-in amplifier performs a very important function in the over-all system.

This unit provides ten (10) selectable output time constants, from 1 msec. to 30 seconds and a connection for external low pass filters. It also furnishes the 1,000 Hz 50%-duty-cycle square wave, and a phasing control, for operation of the radiometer input signal Modulator. The  $\pm 45$  degrees of phase shift, available in the phasing control, permits easy synchronization of the Modulator Switch and coherent detector located in the Lock-In Amplifier.

The full scale sensitivity of the Lock-In Amplifier is 100 microvolts. It has a 24-hour stability of  $\pm 0.2\%$  of full scale.

#### 3.4.5 RADIOMETRIC DATA SYSTEM

The Radiometric Data Acquisition System (RDS) was designed to acquire, digitize and record data from the microwave radiometer. Data is stored on conventional Phillips magnetic tape cassettes.



The electronics and the cassette recorder are housed in a portable cabinet. The system can output its data to a local teletype or to a remote computer using a Bell 202C data set.

This Section describes the system, its accuracy, data storage capacity and modes of operation.

The RDS has been designed with modern integrated circuits using 7400 series TTL with some medium scale integrated circuits to minimize the component count. All units are standard plug-in components to facilitate field repair when necessary.

All data is recorded in a serial digital format which conforms to the ASCII standard for asynchronous data.

Each character is recorded serially on an incremental cassette recorder which always records the bits of each character at its maximum bit rate. The model 133 tape recorder accepts a 300-foot certified Phillips cassette and records both the data and the data complement on two tracks for redundancy.

The RDS system block diagram is shown in Figure 3-5, which shows the interconnections of all major components. This description will explain the interaction of the major components.

**Radiometer** - The radiometer outputs a signal which has a full scale range of zero to +10 volts but uses a smaller portion of that range during actual data acquisition. An output variation of  $0.1^{\circ}\text{K}$  corresponds to a 10 millivolt (mv) change in output voltage.

The RDS is designed to have an absolute accuracy of  $\pm 2$  mv and a resolution of 1 mv. A peak-to-peak noise output of 60 mv must be averaged to detect the desired  $0.1^{\circ}\text{K}$  changes in radiometer output.

**Analog to Digital Converter (ADC)** - A 16-bit decimal, integrating ADC was selected. The unit employs very stable voltage-to-pulse count conversion with a basic accuracy of 0.01%. In order to integrate interfering 60 Hz noise, the unit integrates each data sample for 16.7 ms.

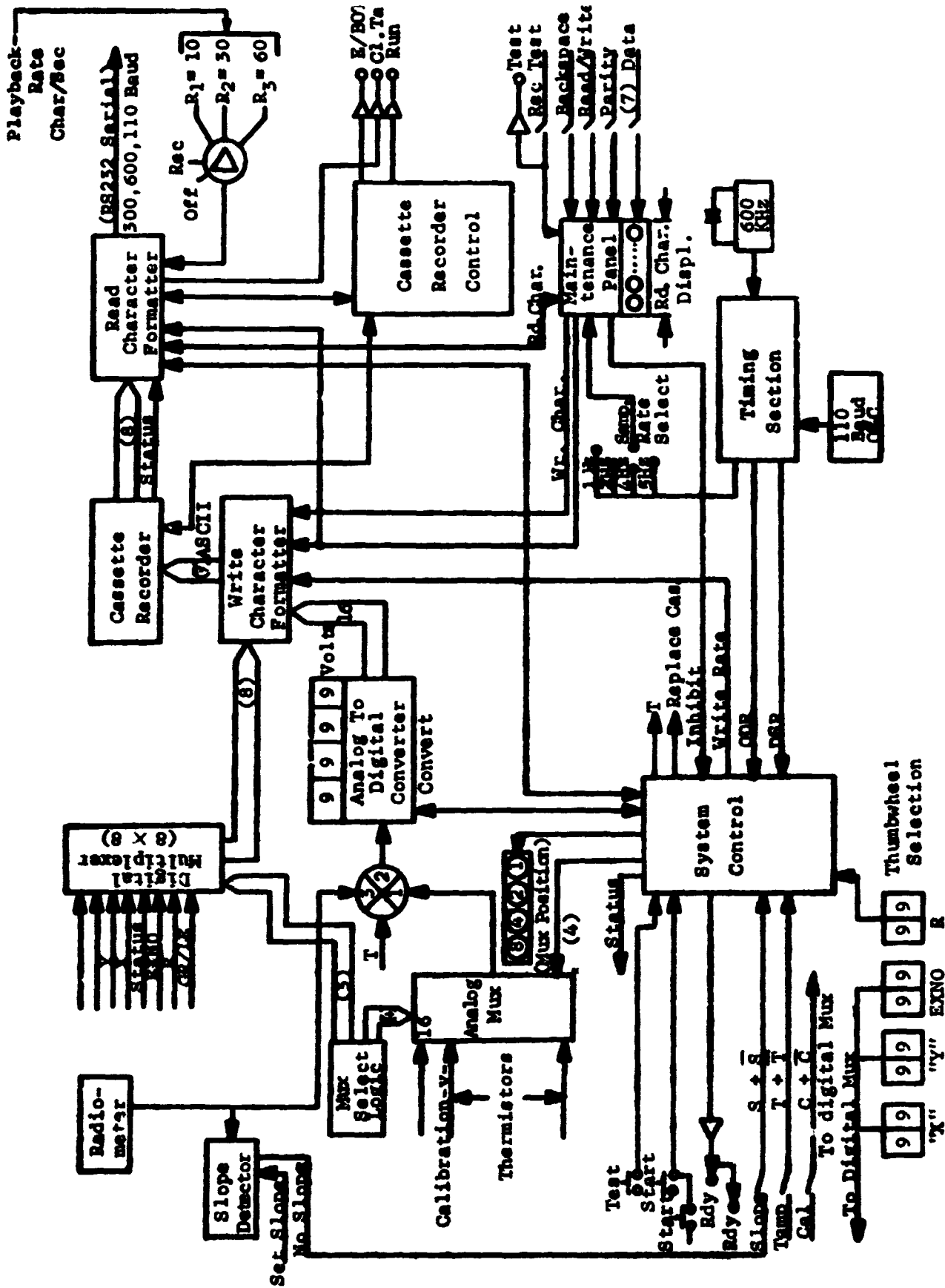


Figure 3-5 - Functional Block Diagram of Radiometric Data System

The ADC has a high impedance differential amplifier which is preceded by an operational amplifier, used for voltage scaling to accommodate the 0 to +10 volt radiometer output signal. Normally, the radiometer is connected to the ADC and is constantly being digitized at one of the four rates (1, 2, 4 or 5 samples per second) selected by a rotary switch located on the maintenance panel. An operator can connect the radiometer, energize the RDS and make any adjustments that are necessary while watching the ADC output.

**Analog Multiplexer** - Solid state differential multiplexing is used in the RDS to connect thermistors and calibration voltages to the ADC. A 16-channel analog multiplexer is used with a 2-channel multiplexer; the latter is shown as a circular switching symbol in the block diagram. Whenever the RDS user selects Temperature (T) (ref.  $T + \bar{T}$  line to system control) port #1 is connected to port #2 and the Analog MUX (16-channel unit) is connected to the ADC.

System control advances the Analog MUX through its 16 positions in response to a start command when (T) is selected, or one step at a time in the TEST mode. The section labelled Analog MUX also contains the constant current generator that forces 237.9 microamperes through the thermistors as each one is connected. Each thermistor is nominally 1,471 ohms at 35°C, which is displayed as 0.350 volts on the 4-digit display.

**MUX Select Logic** - The Mux Select Logic (MSL) operates under the direction of System Control (SC) to deliver the correct binary address to both the analog and digital multiplexers. Logic within the multiplexers accomplish decoding from binary to 8 lines or 16 lines.

**System Control** - The system control (SC) logic contains the logic microprogram to operate the system in the following manner.

In response to a start command, the RDS records the eight digital words inputted to the digital multiplexer as 16 ASCII characters. If T is selected the 16 analog MUX inputs are also digitized and recorded.\* SC then proceeds

---

\*Header and T data are recorded at 60 characters per second regardless of the sampling rate selected.

to record radiometer samples at the selected sampling rate until the number (0-99) of samples specified by the (R) thumbwheels have been digitized. SC finally ends the data sequence and lights the RDY light.

If slope (S) is selected, the RDY light is not lit as long as the radiometer input is varying by more than the slope limit (ref. SET SLOPE). As soon as the radiometer has stabilized (NOSLOPE) SC lights RDY and the sequence can be started. The SC uses a precision 600 KHz crystal oscillator which is contained within the ADC unit as its basic logic timing reference.

SC accepts digital sampling rate (DSR) and output data rate (ODR) signals from the timing section. It uses these signals to derive the correct character writing rate for the character formatter and the conversion rate which is one-fourth of the former (i.e. there are four characters generated for each sample conversion).

SC receives an inhibit signal from the maintenance panel when the recorder is being tested (RECTEST). This causes SC to inhibit its normal cycle when START is depressed. SC creates a signal called "replace cassette" which it derives from the situation where the RDS is in the record mode and End of Tape (EOT) is sensed. The operator recognizes this condition by observing EOT with the tape recorder in the record mode and takes the appropriate action by replacing the cassette.

**Write Character Formatter** - The write character formatter (WCF) accepts 4-bit BCD characters and adds the correct 5, 6 and 7th bits to make each character conform to ASCII format. Each character received by the recorder is then converted to an 8-bit word with odd parity by the R133 recorder.

Whenever the ADC is presented with an overscale input (>9.99v) it records a question mark for the most significant digit (?XXX). When receiving data from the digital multiplexer it accepts 8-bit data words and demultiplexes them into four bit bytes, adds the correct three most significant bits and records the resulting 7-bit word.

**Cassette Recorder** - An incremental, serial cassette recorder Model #133 manufactured by Memodyne is used as the data storage element. Its salient characteristics are:

<b>Tape length</b>	300 feet
<b>Bit Packing Density</b>	240 Bpi
<b>Storage Capacity</b>	72,000 - 8-bit characters
<b>Read/Write speed</b>	60 char/sec.
<b>START/STOP Time</b>	3 ms and 7 ms (resp)
<b>No. Tracks</b>	Two
<b>Record Format</b>	NRZI - redundant
<b>Error Rate</b>	1 bit in $10^7$

All commands to, and data formatting for, the R133 are accomplished in the RDS logic. The only function that an operator can perform directly on the transport is rewind and this is done automatically when the cassette is inserted.

**Cassette Recorder Control (CRC)** the CRC is the control interface to the R133 and operates with the character formatter to control the recorder and to output data. CRC conditions the E/BOT and RUN signals from the tape recorder and the clean tape (CT) signal derived from the read character formatter.

**Read Character Formatter (RCF)** - The RCF accepts parallel characters from the R133 recorder which assembles each group of 8 bits into a parallel output. RCF then adds a start and a stop bit to the character and outputs the data as a serial, RS-232 compatible, character to either a Bell 202C modem or a teletype at one of the selected playback rates.

Although the playback character rates are 10, 30 and 60, their corresponding baud rates are not uniform multiples because the teletype (model ASR-33) requires a 110 baud output. The rate requirements are listed below.

<u>Character Rate</u>	<u>Baud Rate</u>
Rate 1    10 Hz	110
Rate 2    30 Hz	300
Rate 3    60 Hz	600

Rates 2 and 3 involve 10-bit characters with one start and one stop bit while Rate 1 requires 2 stop bits. While the 300 and 600 character per second rates are derived from a crystal oscillator, the 110 baud rate is produced by a small auxiliary oscillator as shown in the block diagram.

**Clean Tape Logic** - When the RDS is used to playback data from a cassette that is not completely full, it is desirable to terminate the transmission as soon as possible to minimize playback time. In order to do this the RCF has "clean tape" logic which operates in the playback mode and detects the fact that the playback head is now looking at clean tape.

The clean tape logic uses the fact that a read start pulse is not followed by tape clock signals when the tape is clean. At any playback speed the tape clock pulses will occur within 3 milliseconds of the start pulse so the logic for clean tape is:

$$\text{CLEAN TAPE} = \overline{\text{TAPE CLOCK}} \text{ for Approx. } 10 \text{ ms}$$

The effect of clean tape (CT) is to extinguish the run mode by clearing the run flip-flop.

**Maintenance Panel (MP)** - The MP contains the necessary controls and displays to bypass the RDS front-end in order to record a test character on tape. There are also eight data lights to display characters that can be read one at a time while moving forward or backward.

The recorder test switch REC TEST contained on the MP is used to place the system in that mode. This control and the sampling rate selector are really system function switches but are located on the maintenance panel to simplify the RDS front panel.

**Timing Section (TS)** - The TS contains the necessary frequency divider logic to reduce the 600 KHz reference clock signals to pulse rates which are applicable to the RDS operation. Sampling rate selections are made by selecting rates which exist in the TS logic. The TS logic also transmits the correct data sampling rate (DSR) and output data rates (ODR) to the SC.

**Data Storage Capacity** - The RDS can record 72,000 asynchronous characters on one 300-foot cassette. Since a fixed-length header is recorded prior to each data record, and the number of temperatures and calibration points are fixed when selected, an equation can be developed to describe the RDS data storage capacity.

A convenient parameter is the number of data blocks where one block is defined as all of the data between two headers.

$$\text{No. of Data Blocks} = \frac{72 \times 10^3 \text{ characters}}{16N + \sum_{n=1}^N 4R_n + 64T_n}$$

In the above expression, the variable  $R_n$  can be 1 to 99 for each value of  $n$ . The value of  $R$  is determined by two thumbwheel switches labeled  $R$  that are mounted on the RDS front panel. A single toggle switch marked  $T$  and  $\bar{T}$  determines the value of  $T_n$  as 0 or 1. The minimum number of data blocks that can be recorded is given by the case where the user always selects temp. and 99 radiometer samples. A "more-likely" case is where the user selects the temperature ( $T$ ) data ten percent of the time and records 20 data points. Both values are calculated as follows:

$$(\text{No. of Blocks})_{\min} = \frac{72 \times 10^3}{N(16 + 396 + 64)} = \frac{72 \times 10^3}{476N}$$

The largest integer value for  $N = 151$  which gives:

$$(\text{No. of Data Blocks})_{\min} = 151$$

$$\begin{aligned} (\text{No. of Data Blocks})_{\text{ave}} &= \frac{72 \times 10^3}{16N + \frac{N}{10}(64) + 4(20)N} \\ &= \frac{72 \times 10^3}{102.4N} \end{aligned}$$

$$(\text{No. of Data Blocks})_{\text{ave}} \approx 700$$

### 3.5 RADIOMETER CALIBRATION

The purpose of the radiometer calibration was to determine the relationship between output voltage and input noise temperature, to assess the linearity of the radiometer response, to calibrate the internal noise tube, and to measure radiometer sensitivity. A hot-cold standard noise generator was used in the calibration. The noise generator uses two resistive elements, one immersed in liquid nitrogen (77.3°K) and the other mounted in a temperature-controlled oven (373.2°K). The output of the noise generator was connected to a variable attenuator via an RF cable. The antenna was removed and an RF cable from the variable attenuator was connected directly into the radiometer. The radiometer input brightness temperature,  $T_B$ , can be computed using the radiative transfer equation,

$$T_{out} = T_L + (T_{in} - T_L) (10^{-\gamma/10}) \quad (3-7)$$

where,

- $T_{in}$  = resistive load input brightness temperature (°K)
- $T_L$  = resistive load temperature (°K)
- $T_{out}$  = resistive load output brightness temperature (°K)
- $\gamma$  = resistive load attenuation (db)

Initially, setting  $T_{in}$  equal to the brightness temperature of the noise generator and, given the temperatures and attenuations of the three loads, consisting of two RF cables and variable attenuator, Equation (3-7) can be solved iteratively for the three loads to yield  $T_B$ .

The calibration procedure was to record,

- 1) The temperatures of the two RF cables and variable attenuator
- 2) The variable attenuator setting and
- 3) A series of 100 radiometer output readings (measured in volts) at a rate of one reading per second.



An average  $V_0$ , and rms variation  $\Delta V_0$ , of the 100 readings was then found. Periodically, the radiometer was switched to the Zero and Calibrate modes. In the Zero mode the radiometer was looking at the internal base load, and in the calibrate mode it was looking at the internal noise tube. As in the operate mode, 100 readings were taken and  $V_z$ ,  $\Delta V_z$ ,  $V_c$ , and  $\Delta V_c$  were found. Figure 3-6 shows  $(V_0 - V_c)$  plotted against  $T_B$  which was computed from Equation (3-7). Each point corresponds to a different variable attenuator setting for which  $V_0$  was measured.  $V_z$  was essentially constant, varying by less than 1%. The radiometer response is very linear. Since we were particularly interested in the radiometer response at the higher temperatures, a linear fit, based on a least-squares approximation, was found using the nine points corresponding to the nine highest  $T_B$ 's. The fit was,

$$V_0 - V_z = 0.05372 T_A - 16.57 \pm 0.01 \text{ mv} \quad (3-8)$$

where,  $\pm 0.01 \text{ mv}$  is the rms deviation from a straight line. Noting that the range of  $T_B$  over the nine points was  $70^\circ\text{K}$ , the uncertainty in the slope of the line is  $0.01 \text{ mv}/70^\circ\text{K}$ . The gain,  $G$ , of the radiometer is given by the reciprocal of the slope:

$$G = 18.62 \pm 0.05 \text{ }^\circ\text{K/mv} \quad (3-9)$$

The difference  $(V_c - V_z)$  during the calibration was  $2.65 \text{ mv}$ . Multiplying this figure by the gain gives the amplitude of the pulse from the noise tube in  $^\circ\text{K}$ . The noise tube calibration pulse was  $53.1 \pm 0.1^\circ\text{K}$ . Assuming this pulse stays constant, the figure can be used in subsequent experiments to determine  $T_B$  by means of the equation,

$$T_B = 53.1 \left( \frac{V_0 - V_z}{V_c - V_z} \right) + T_{\text{base}} \quad (3-10)$$

where,

$T_{\text{base}}$  is the temperature of the base load.

The sensitivity,  $\Delta T_B$ , of the radiometer is defined as the rms fluctuation of the radiometer output, in the absence of an input signal, in  $^\circ\text{K rms}$ .

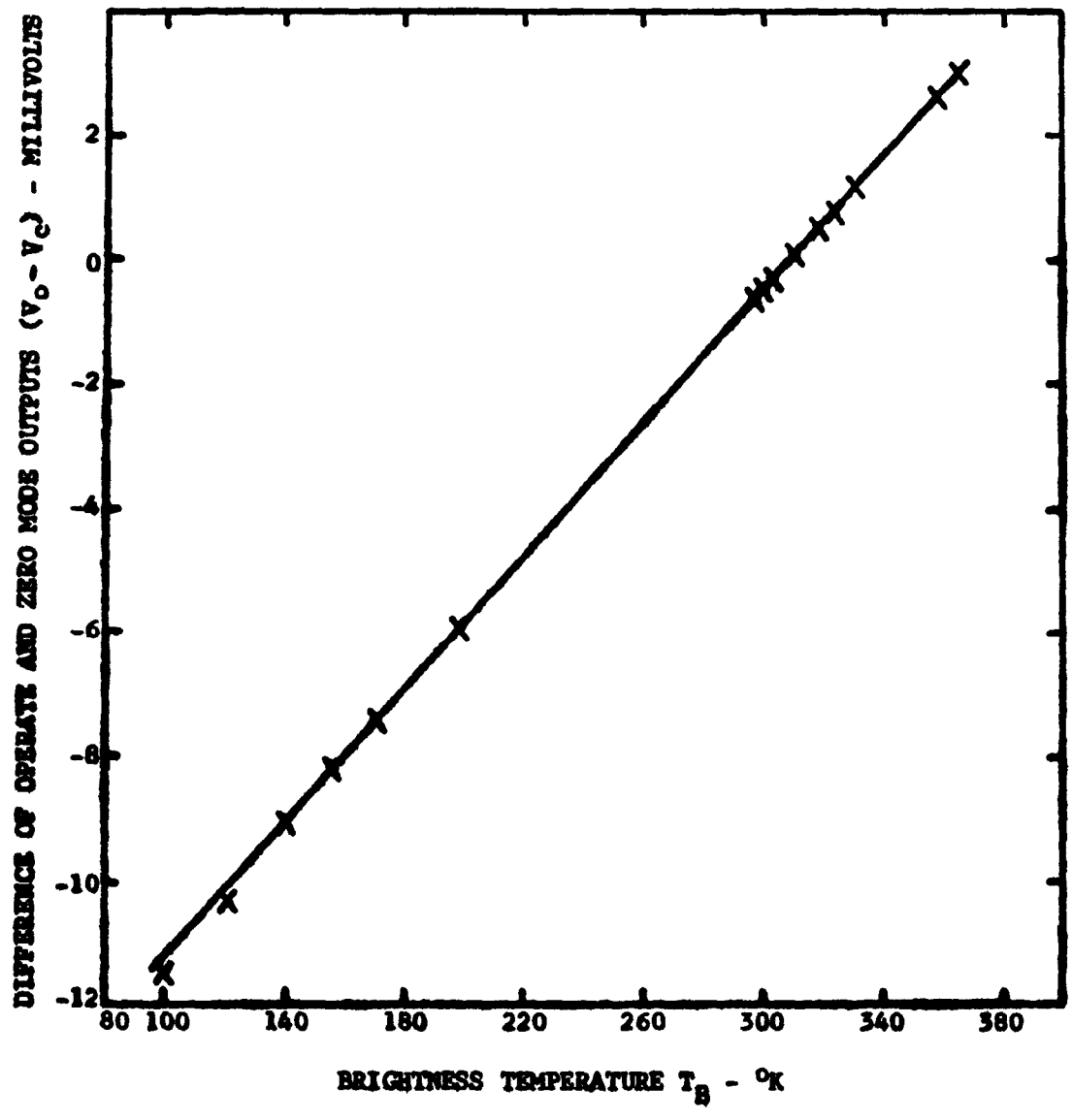


Figure 3-6 - Radiometer Calibration Data

$$\Delta T_B = G \Delta V_0, \text{ } ^\circ\text{K rms} \quad (3-11)$$

$\Delta T_B$  was found to be close to  $0.05^\circ\text{K}$  in the calibration experiment, in which a 10-second time constant was used.

### 3.6 DATA REDUCTION

The radiometric data acquisition system (RDS) acquires and digitizes data on magnetic tape using a conventional Phillips data cassette. All data is recorded in a serial digital format which conforms to the ASCII standard for asynchronous data. The data is grouped into 'runs', with carriage return and line feed characters separating the runs. Each run consists of the following data:

- (1) Number of radiometer samples (1-100)
- (2) Experiment number (00-99)
- (3) Sampling rate (1, 2, 4, 5 samples/sec)
- (4) Status (specifies radiometer mode and if temperatures were recorded)
- (5) A 4-digit number (for specifying time, attenuation, or other pertinent information)
- (6) Thirteen temperature probe measurements (if recorded)
- (7) Series of radiometer samples.

The processing of this data was performed through National CSS, a time-sharing computer network using five IBM System 360 Model 67 processors.

The existing NCSS software PTFILE, used for inputting asynchronous data, required that a carriage return and line feed occur after every 140 characters, or less. This constraint required that the data recorded on the cassette first be edited. Because the cassette could not be stopped in playback mode, a copy of the data was generated on punched paper tape by playing the cassette into a model 35 teletypewriter. This punched paper tape was then played back into the teletypewriter to generate a second punched paper tape. During this second playback, the paper tape reader was interrupted after every 100 characters or so, and carriage return and line feed were manually typed in. These two additional characters appeared on the second punched paper tape, making it compatible with PTFILE.

The edited paper tape was read into the computer on file INPUT1. INPUT1 consisted of a series of records, each record corresponding to the data that was sandwiched between sets of carriage return and line feed characters. Using an NCSS edit command, the character "!" was inserted at the end of the data in each record. The Fortran program SETUP1 was then run. SETUP1 reads INPUT1, checks for errors in the formatting of the data, and blocks the data into separate runs on file INPUT2. File INPUT2 is then read by Fortran program SETUP2 which checks for bad characters in the data field. Any bad characters are deleted and the remaining data is read onto file INPUT3.

Fortran program RADIOM, along with associated subprograms RADEMS and PBTEMP, then read INPUT3. Thirteen titles, each consisting of 40 characters or less, are next inputted from the teletypewriter console into RADIOM. These titles serve to identify the thirteen temperature probes. RADIOM converts the temperature probe voltages to °C, finds the mean and rms values of the series of radiometer samples, determines how well the samples agree with a random process, using the chi-square test, and uses Equations (3-10) and (3-11) to compute the apparent temperature  $T_A$  and rms noise  $\Delta T_A$ , based on previous zero and calibrate mode readings. This information, along with items 1 through 5 listed on the previous page, is printed out as shown in Figure 3-7. RADIOM also outputs onto file 03 the probe temperatures and, onto file 04, the mean and rms values of the radiometer samples and the chi-square test result. Listings of programs SETUP1, SETUP2, RADIOM, and subprogram PBTEMP and RADEMS are in Appendix A.

\* \* \* RDS READ OUT \* \* \*

EXPERIMENT NUMBER = 7  
TIME = 04:21

RADIOMETER IN OPERATE MODE  
TEMPERATURES RECORDED

SAMPLE RATE = 1/SFC  
NUMBER OF RADIOMETER SAMPLES = 100

RDS CALIBRATION		
ZERO	PROBE SCALE	FULL SCALE
2	2352	9997

PROBE TEMPERATURES (DEG C)

R1 = ROOM AIR	=	25.6 C
R2 = BASE LOAD	=	37.4 C
R3 = RECTAL	=	36.4 C
R4 = RIGHTSURFACE	=	37.0 C
R5 = LEFT SURFACE	=	24.3 C
R6 = RIGHT ONE INCH DEEP	=	37.9 C
R7 = RIGHT ONE-HALF INCH DEEP	=	37.9 C
R8 = NOISE SOURCE INPUT PORT	=	34.9 C
R9 = RIGHT SUBCUT.	=	37.3 C
R10 = LEFT ONE-HALF INCH DEEP	=	27.8 C
R11 = LEFT SUBCUT.	=	26.2 C
R12 = LEFT ONE INCH DEEP	=	27.5 C
R13 = ROOM AIR	=	26.4 C

MEAN RADIOMETER OUTPUT = 2942.5  
RMS DEVIATION = 14.1  
CHI-SQUARE TEST = 0.243E 00

APARENT TEMPERATURE = 305.57 DEG K  
RMS NOISE = 0.15 DEG K  
BASED ON CALIBRATION AT TIME = 04:10

Figure 3-7 - Sample Computer Printout of Radiometric and Temperature Probe Data, for Final Dog Experiment

## Section 4

### TEMPERATURE MEASUREMENTS ON DOGS

#### 4.1 MEASUREMENTS ON FIRST DOG

An investigation was conducted on a large mongrel dog, at the New England Medical Center Hospital, to attempt to determine the relationship between blood flow and surface and subsurface temperatures. This work involved the radiometric data system (RDS) only, with a variety of temperature probes and a flowmeter; the radiometer proper was not employed in these initial observations. Dr. W. Carney, of the Hospital staff, assisted with this experiment.

The dog was anesthetized and the following temperature probes were installed in the inner thigh of each hind leg: surface, subcutaneous, 0.95 cm deep and 1.9 cm deep. The dog's abdomen was opened and a Carolina Medical Electronics, Inc., square-wave electromagnetic flowmeter was attached to the right iliac artery, leading to the test leg. The right iliac was then clamped shut and temperatures were recorded.

The results are shown in Figures 4-1 and 4-2. It should be noted that the initial downward trend of temperatures in both legs is mainly due to the cooling effect of the laboratory air conditioner; the room temperature had risen to a level of 82°F. The important feature, in the four pair of plots, is the difference in temperature between the reference and test legs. Thus, after 0.5, 1.0 and 1.5 hours, the drops in the test leg temperatures were as listed in Table 4-1.

Table 4-1

#### TEMPERATURE DROPS IN TEST LEG

Probe Depths	After 0.5 hr.	After 1 hr.	After 1.5 hrs.
1.9 cm	0.65°C	0.76°C	0.90°C
0.95 cm	0.60	1.05	1.50
Subcut.	1.70	2.40	3.20
Surface	0.80	1.40	2.00

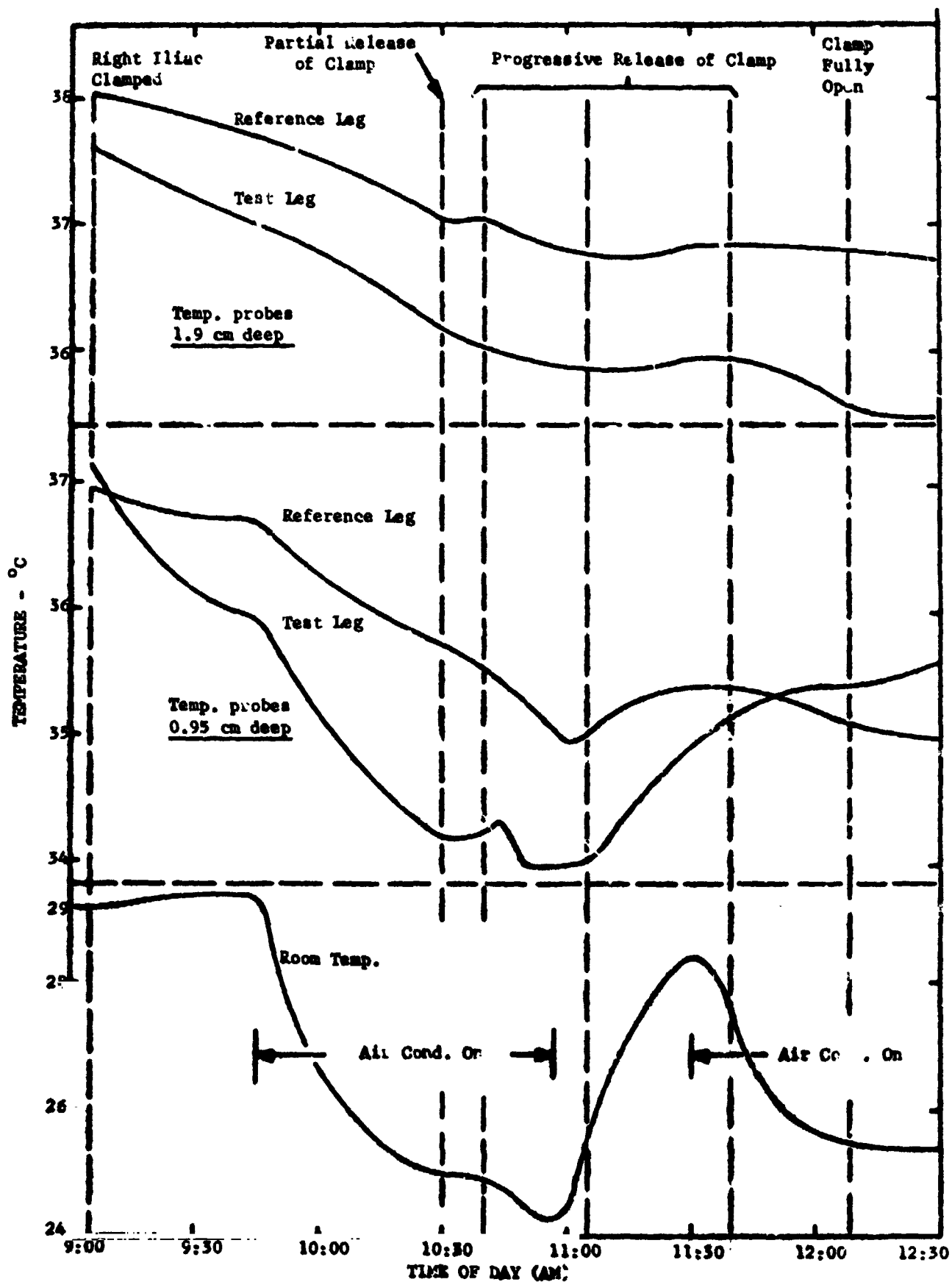


Figure 4-1 - Dog's Leg Temperatures versus Time

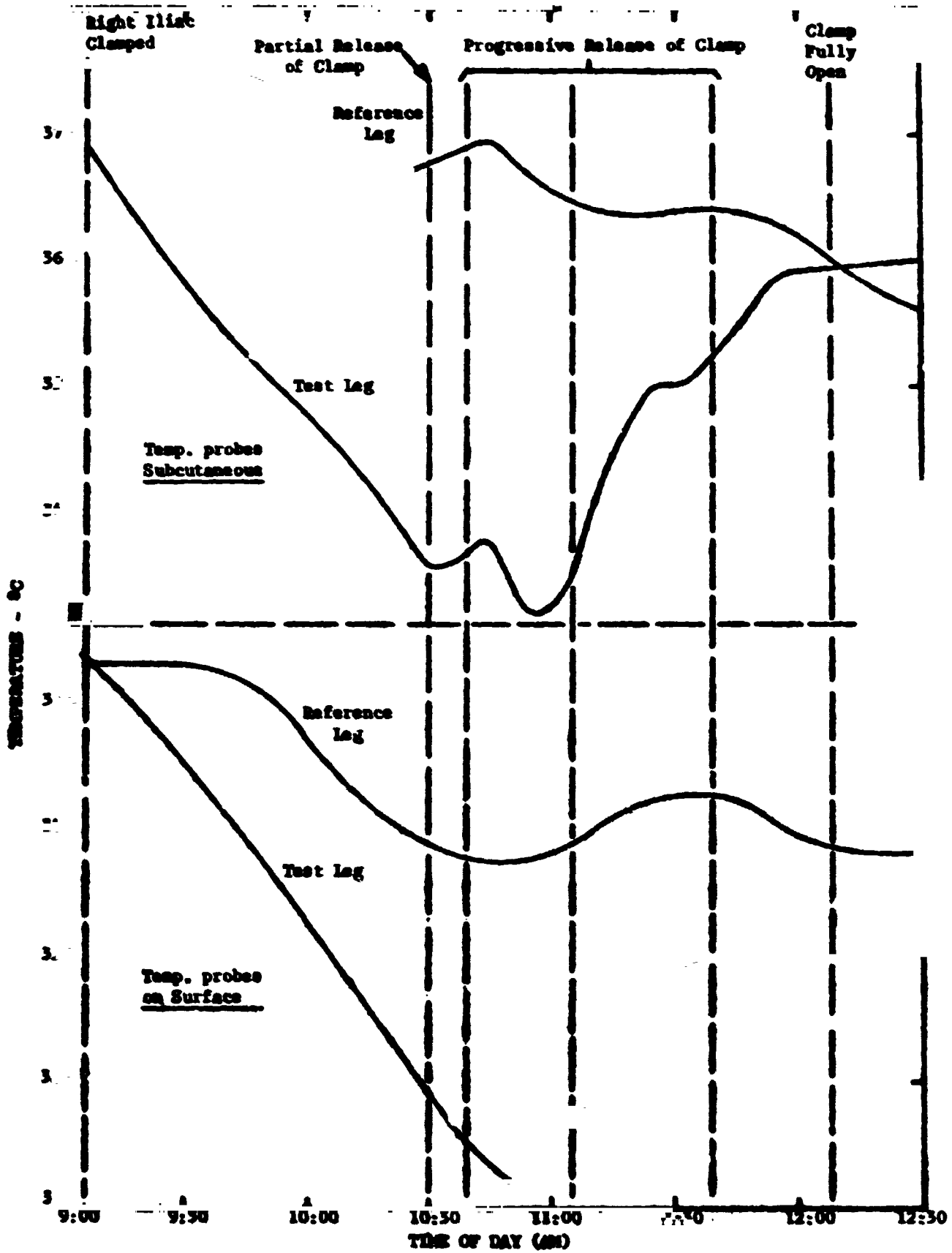


Figure 4-2 - Dog's Leg Temperatures versus Time



The above data shows the largest drops in the subcutaneous probe, with the surface probe being the next largest. The drops at the 0.95 cm depth are not too far removed from those at the surface. It should be noted, however, that collateral circulation would tend to compensate, to a considerable extent, for blood cutoff in the iliac artery. Thus, the above temperature drops are quite encouraging.

It is difficult to explain the continued increase in test leg temperatures, for the 0.95 cm and subcutaneous depths, after 11:45 am; the corresponding reference leg temperatures were decreasing after this point in time. It appears that the increased blood flow had a greater effect at these depths than at the surface and 1.9 cm depth.

Unfortunately, the readings furnished by the electromagnetic flowmeter were somewhat erratic; thus, the blood flow in the right iliac could not be determined.

#### 4.2 MEASUREMENTS ON SECOND DOG

A large mongrel dog, similar in size to a German Shepherd, was anesthetized and prepared for nighttime radiometric observations, after the UHF TV stations had gone off the air, to avoid TV interference with the radiometer. Temperature probes were installed in the thighs of the hind legs as follows: surface, subcutaneous, 1.3 cm and 2.6 cm. Instead of clamping off the right iliac, as in the experiment described in the above Paragraph, a tourniquet was applied to the upper thigh of the right leg. It was expected that this would reduce collateral circulation and the flow in the arteries would also be smaller; it was also expected that a faster temperature response would be achieved. A Statham Model M-4001 Square-Wave Electromagnetic Flowmeter was arranged for use in this experiment. Dr. W. Carney was in attendance during this investigation.

Prior to applying the tourniquet, voltage standing wave ratios were measured with the antenna disconnected from the radiometer and placed on the dog's right leg. The average value was 2.6:1, across the radiometer bandwidth. It can be shown that, for this value, the antenna power transmission is 0.8 (see Section 5.2).

Following this procedure, the antenna was re-installed on the radiometer and placed in close contact with a cleanly shaven area near the probes on the right leg. Temperatures were, next, recorded on both legs and the tourniquet applied as tightly as possible to the upper thigh of the right leg. Radiometer readings were taken and temperatures recorded for a period of 30 minutes. Figure 4-3 shows that the resultant radiometer apparent temperatures dropped 1.7°K during this period. Thermodynamic temperature changes, recorded during this period, are listed in Table 4-2.

Table 4-2

TEMPERATURE CHANGES IN REFERENCE AND TEST LEGS

Probe Depths	Ref. Leg Temp. Change (30 min.)	Test Leg Temp. Change (30 min.)
2.6 cm	- 0.5°C	- 1.1°C
1.3 cm	- 0.4	- 2.1
Subcutaneous	- 0.3	- 1.7
Surface	No reading (probe fell off)	- 2.1
Room temperature change: + 0.4°C		

Many more readings were taken over a period of 5.5 hours; however, unfortunately, all of the data was lost due to numerous spurious characters recorded by the radiometric data recording system (RDS). This was caused by overheating of the magnetic tape recorder. The above sample data was recorded manually from the RDS display. Based on these results, it is probable that the radiometer sensed subsurface temperature changes from a depth of, at least, 1.3 cm.

The flowmeter probe was applied to the femoral artery and vein in the test leg, during the above observations. A rigid plastic tube was placed around these blood vessels and the tourniquet was placed over the tube and around the thigh of test leg.

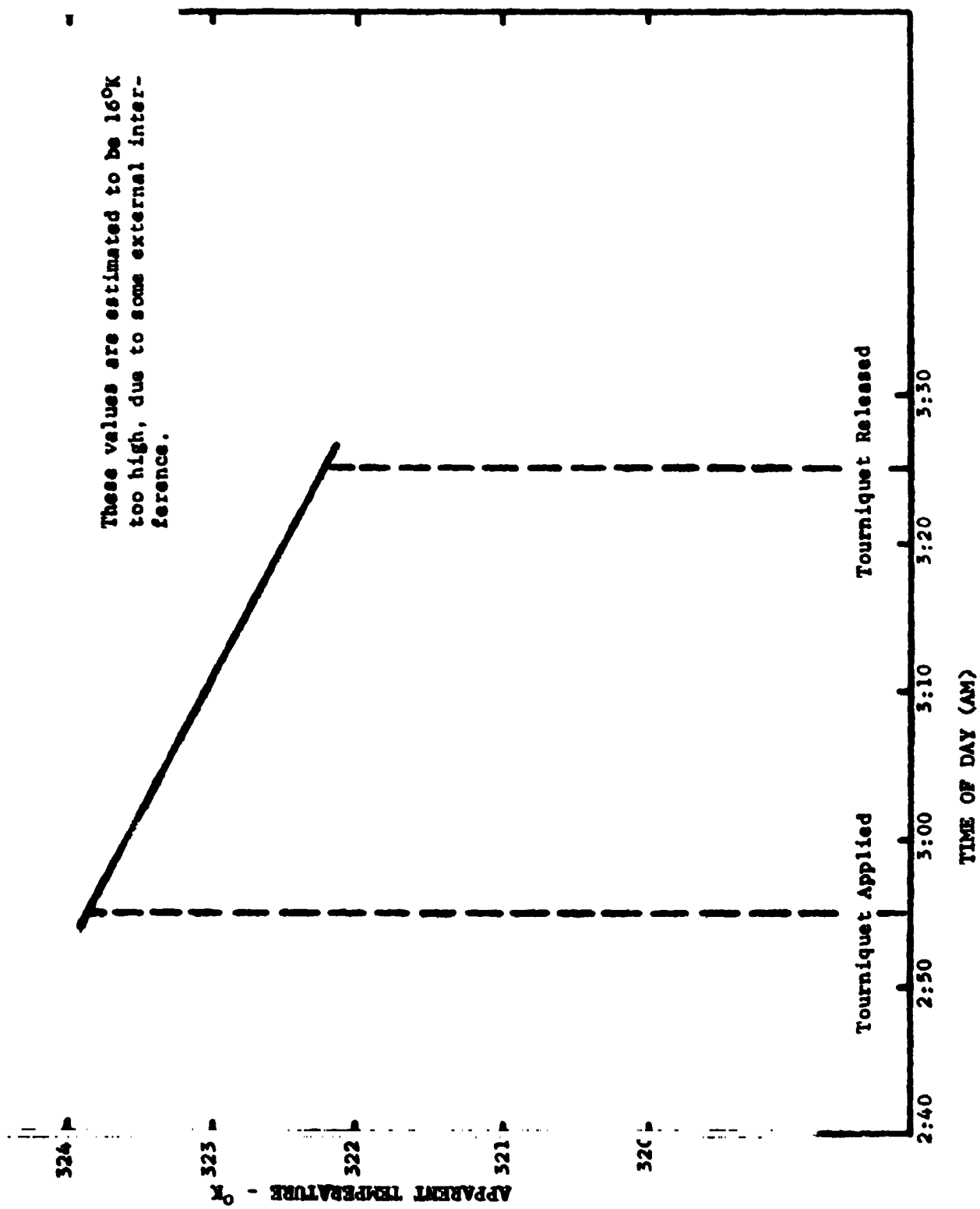


Figure 4-3 - Radiometric Apparent Temperature versus Time

Figure 4-4 shows the flowmeter readings versus time. The tourniquet was applied at 5:25 am; however, the flowmeter did not show any drop in blood flow until the femoral artery was clamped shut at 6:25. When the clamp was opened 5 minutes later, the flowmeter readings gradually rose to a rather high value of 108 ml/min., and then began dropping to 66 ml/min., with no other changes made in the experiment setup. Due to the unpredictable nature of the readings, the flowmeter was not used in any further measurements.

The discouraging results obtained with two different flowmeters suggest that other methods be explored for use in correlative blood flow measurements. It is understood that radioisotope techniques could provide useful information on blood flow for this type of experiment.

#### 4.3 MEASUREMENTS ON THIRD DOG

A large black Labrador male dog, weighing 57 lb., was used in this experiment. The dog was anesthetized with 11 cc of pentobarbital and four (4) temperature probes were attached to, and inserted in, the thighs of each hind leg. Dr. H.H. Miller was in attendance. The right hind leg was chosen to be the test leg. A temperature probe was inserted in the esophagus.

The radiometer was used in making measurements on the test leg; however, due to excessive UHF TV interference, none of the radiometer data was of any value. Nonetheless, the extensive temperature readings, taken during the course of the experiment are of some interest.

Figures 4-5 and 4-6 show temperature readings for various events throughout the 6-hour experiment. Referring to Figure 4-5, it will be noted that, during a 36-minute interval, following clamping of the femoral artery in the test leg, the only significant temperature drop occurred at the surface of the leg. After a tourniquet was applied to the leg, there was a drop of  $1.4^{\circ}\text{C}$  at depths of 1.3 cm and 2.5 cm, over the next 39 minutes. It will be noted that the subcutaneous and surface temperatures increased  $0.6^{\circ}\text{C}$  during this period; this is probably because the room temperature rose by  $2.5^{\circ}\text{C}$  in this interval.

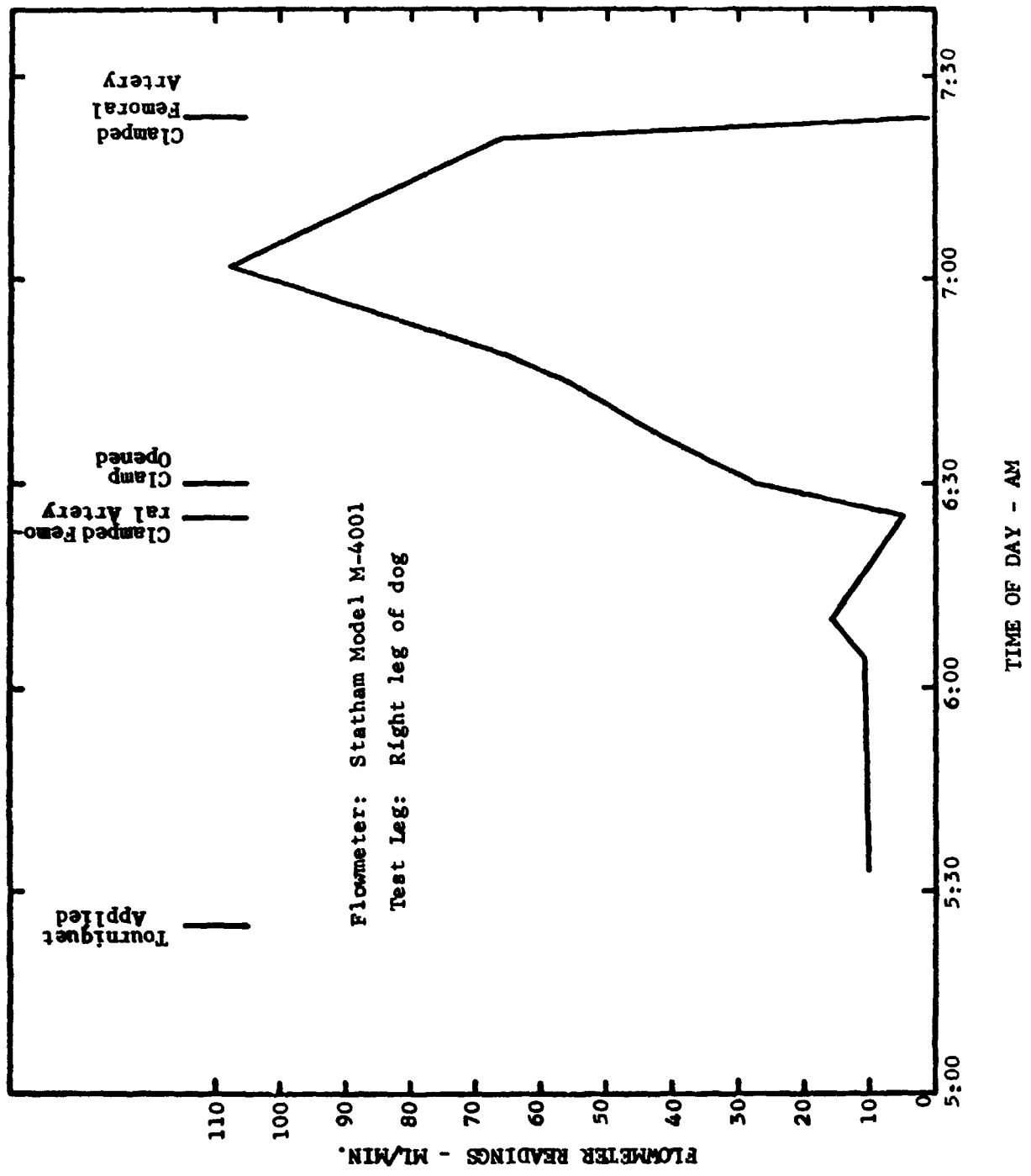


Figure 4-4 - Electromagnetic Flowmeter Readings versus Time, Second Dog

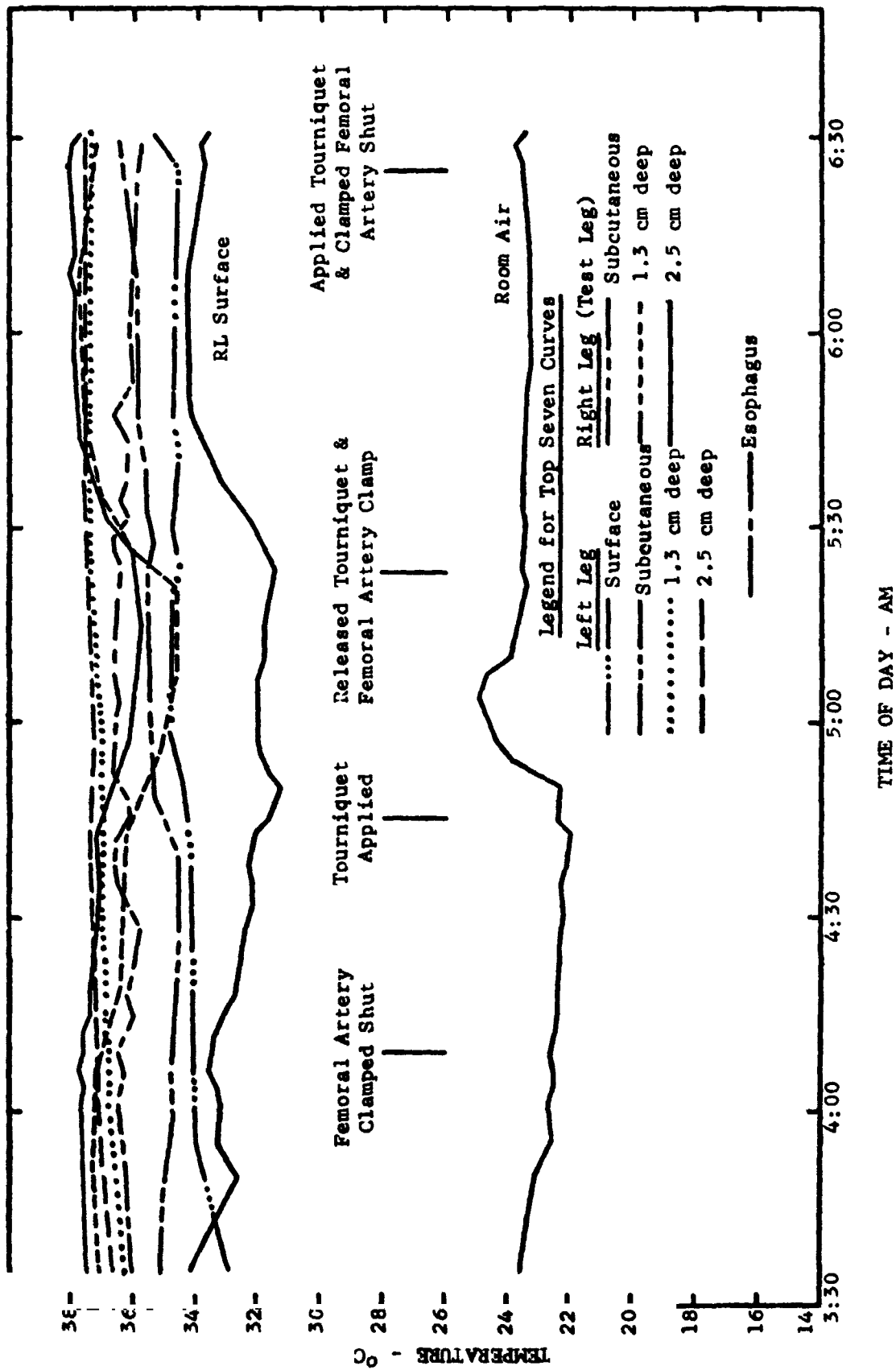


Figure 4-5 - Temperatures versus Time, for Thigh of Third Dog

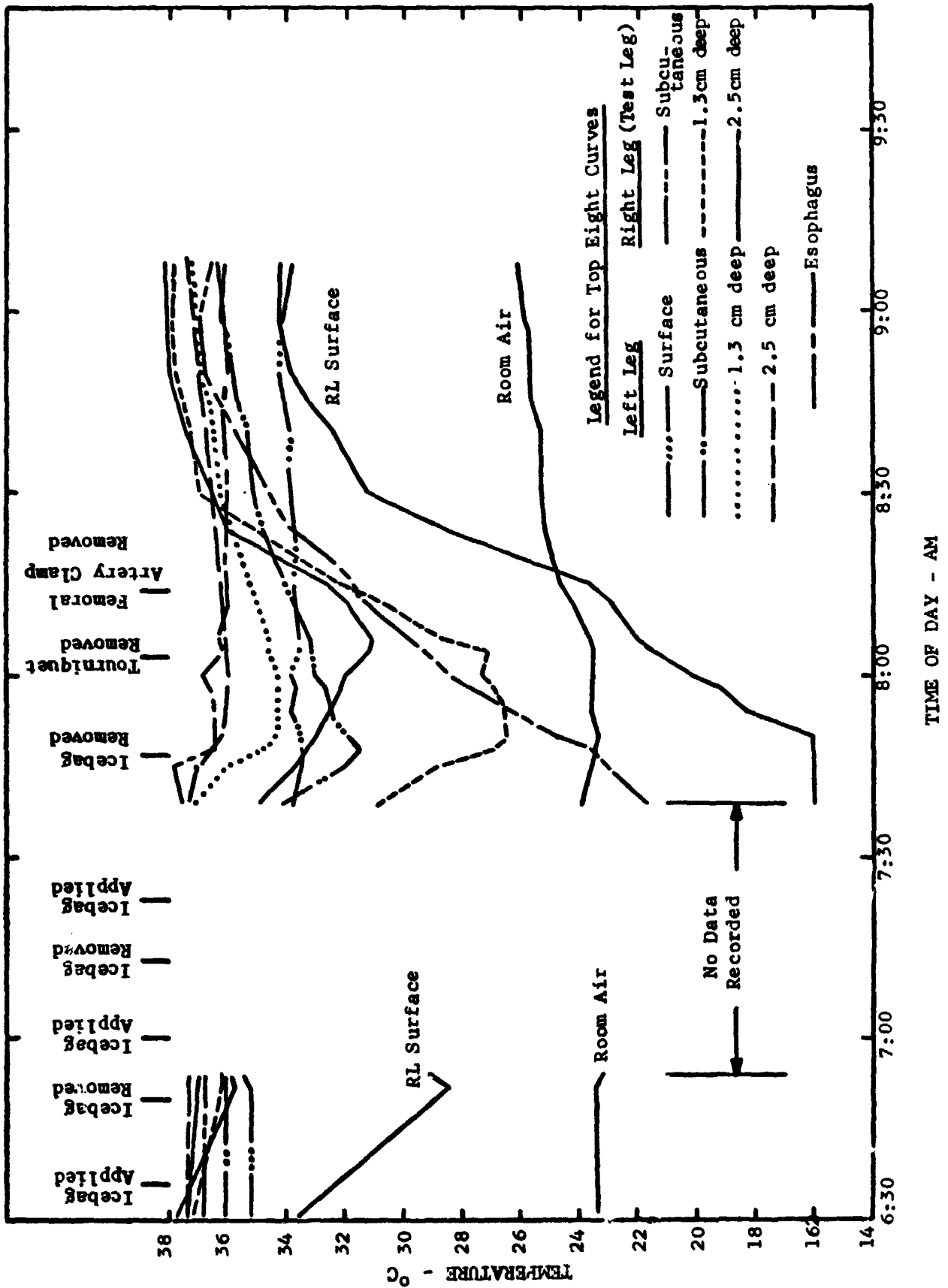


Figure 4-6 - Temperatures versus Time, for Thigh of Third Dog

Following release of the tourniquet and femoral artery clamp at 5:23 am, the surface, 1.3 and 2.5 cm temperatures rose steadily by 3°C over the next 32 minutes; however, the subcutaneous temperature rose only about 0.4°C during this time. It is difficult to explain the latter, except that the blood flow could have been relatively limited in the subcutaneous region, thus retarding a rise in temperature.

Figure 4-6 shows a continuation of the temperature data, obtained under somewhat different conditions, involving the use of a tourniquet, femoral artery clamp and icebag containing an ice-alcohol mixture. Unfortunately, this plot has a data gap in it, due to some equipment problems; however, the effect of the icebag is evidently quite pronounced at the surface and all depths between 7:23 and 7:47 am. The temperature reduction is greatest, of course, at the surface of the test leg and becomes progressively smaller at the subcutaneous, 1.3 cm and 2.5 cm depths, respectively. This is understandable since the effect of a cold body, placed on the surface, would tend to be reduced with increasing depth, due to the thermal insulation afforded by the intervening tissue.

When the icebag was removed, at 7:47 am, the surface and subcutaneous temperatures began to rise while the 1.3 and 2.5 cm temperatures continued to drop for a few minutes. This lag, in reversing the downward trend in temperature, is greater at the 2.5-cm depth. The temperature at this depth finally began to rise 19 minutes after the icebag was removed and 3 minutes after the tourniquet was removed. Thus, the restoration of normal temperatures at depths of 1.3 and 2.5 cm was relatively slow until full circulation was permitted by the removal of the tourniquet. This indicates that very little, if any, collateral circulation was permitted by this device.

The above data shows that an ice mass can be employed quite effectively in establishing conditions suitable for investigations of the heating effects of blood flow at different depths in the body. This technique can be readily and safely adapted to blood flow investigations in humans wherein a microwave radiometer is employed in sensing subsurface temperatures.

Alternatively, a heat pulse could be applied, at the location of interest, with the radiometer measuring the time taken to cool that area. In this connection,



an interesting experiment is described in Reference 3. The technique involves applying a heat pulse to the skin and measuring the rate of blood flow with the aid of two thermistor sensors placed a known distance apart. This method could furnish useful correlative data during radiometric observations.

## Section 5

### RADIOMETRIC OBSERVATIONS

#### 5.1 INTRODUCTION

As discussed in Section 4, early attempts at obtaining radiometric data, on phantom models and blood flow in dogs, were thwarted by excessive externally generated interference. To determine the exact frequencies of the interfering signals, a survey was conducted, in the laboratory and at the New England Medical Center Hospital, using a sensitive spectrum analyzer. Based on information obtained in this manner, suitable bandpass and band-rejection filters were specified and purchased for the radiometer. These included a bandpass filter for use at NASA-Ames. The characteristics of these components were described in Section 3.

Following incorporation of the filters, the radiometer performed satisfactorily for phantom measurements and observations on dogs.

#### 5.2 PHANTOM MEASUREMENTS

Two phantom models were established and measurements were performed on them in the laboratory. Data obtained from the first model indicated an excessive amount of outside RF interference and no conclusive results were obtained. The second phantom, shown in Figure 5-1, was entirely enclosed in a double layer of aluminum foil to eliminate any possible interference. To prevent evaporation the beef fat and lean beef were also wrapped in Saran Wrap. Four temperature probes were inserted at the various depths shown. Radiometer observations were made concurrently with temperature probe measurements as current was gradually applied to both heaters. A 10-second time constant was used, and 100 samples were taken, at a rate of 1 sample/sec., for each radiometer observation. During a 30-minute period, shortly after the beginning of the experiment, a partial short in the heater resulted in the radiometer measurements being in error.

The results of these measurements are shown in Figure 5-2. The highest temperature throughout most of the 2-hour period was shown by a probe at a depth of 5.1 cm, which was the closest to the heaters. Enclosing the phantom in aluminum

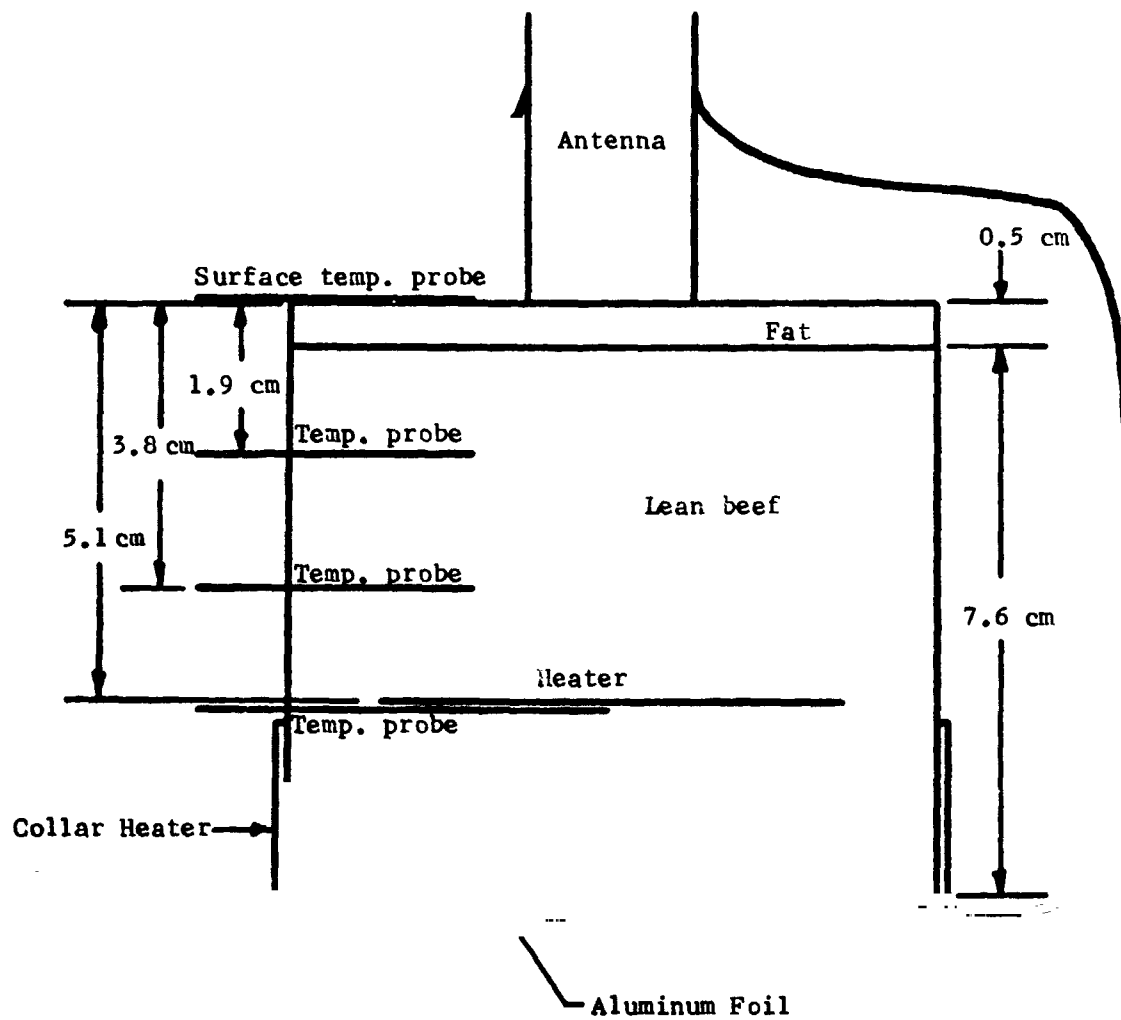


Figure 5-1 - Phantom Model.

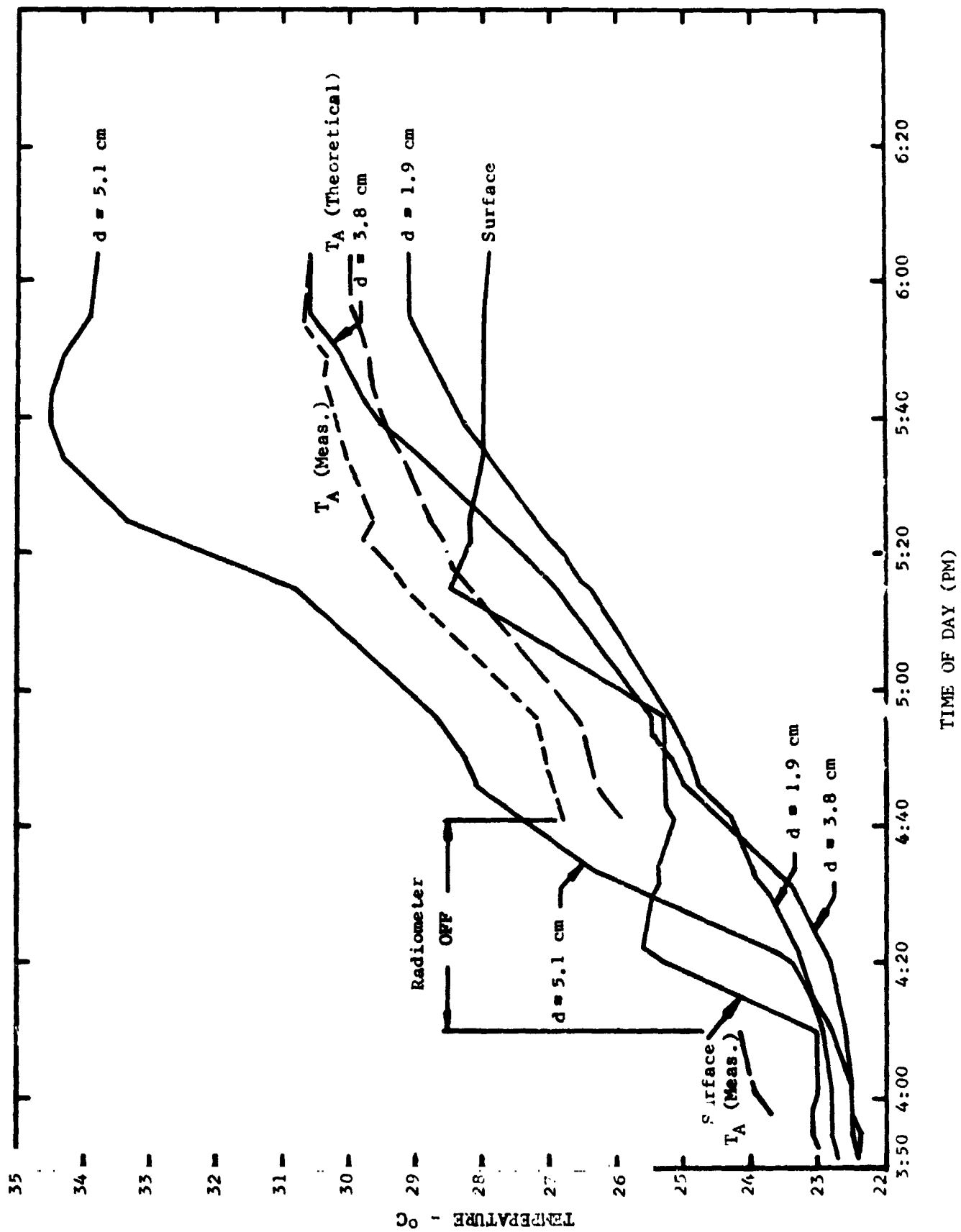


Figure 5-2 Phantom Apparent Temperatures and Temperatures

foil resulted in much of the heat convecting up the sides to the top surface. This caused the surface temperature probe to be warmer, at times, than the 1.9 and 3.8 cm-deep probes. The short-dashed  $T_A$  curve in Figure 5-2 is the measured radiometer apparent temperature given by Equation (3-10). The layer depths shown in Figure 5-1 and the four probe temperatures, given in Figure 5-2, were inputted into program LAYER, discussed in Section 2, along with the appropriate dielectric permittivities; theoretical brightness temperatures,  $T_B$ , and reflectivities,  $R$ , were then computed. Equation (2-1) was then used to derive theoretical apparent temperatures, shown by the long-dashed curve in Figure 5-2. The agreement between the measured and theoretical apparent temperatures is excellent. Considering the uncertainties in specifying permittivities and temperature profiles in the layers, and the fact that the phantom did not have an infinite cross-section (in fact, the phantom cross-section is only a fraction of the free space wavelength), the small 1°K offset between theory and measurement is remarkable.

The effective temperature,  $T_e$ , of a layered medium can be defined by an equation analogous to Equation (2-1).

$$T_A = (1 - R) T_e + R T_R \quad (5-1)$$

or,

$$T_e = T_B / (1 - R) \quad (5-2)$$

The reflectivity,  $R$ , can be determined by measuring the voltage standing wave ratio (VSWR) denoted by  $S$ .

$$R = 1 - \frac{4S}{(S + 1)^2} \quad (5-3)$$

The transmission  $\tau$  is defined as

$$\tau = 1 - R \quad (5-4)$$

and is plotted versus  $S$  in Figure 5-3.

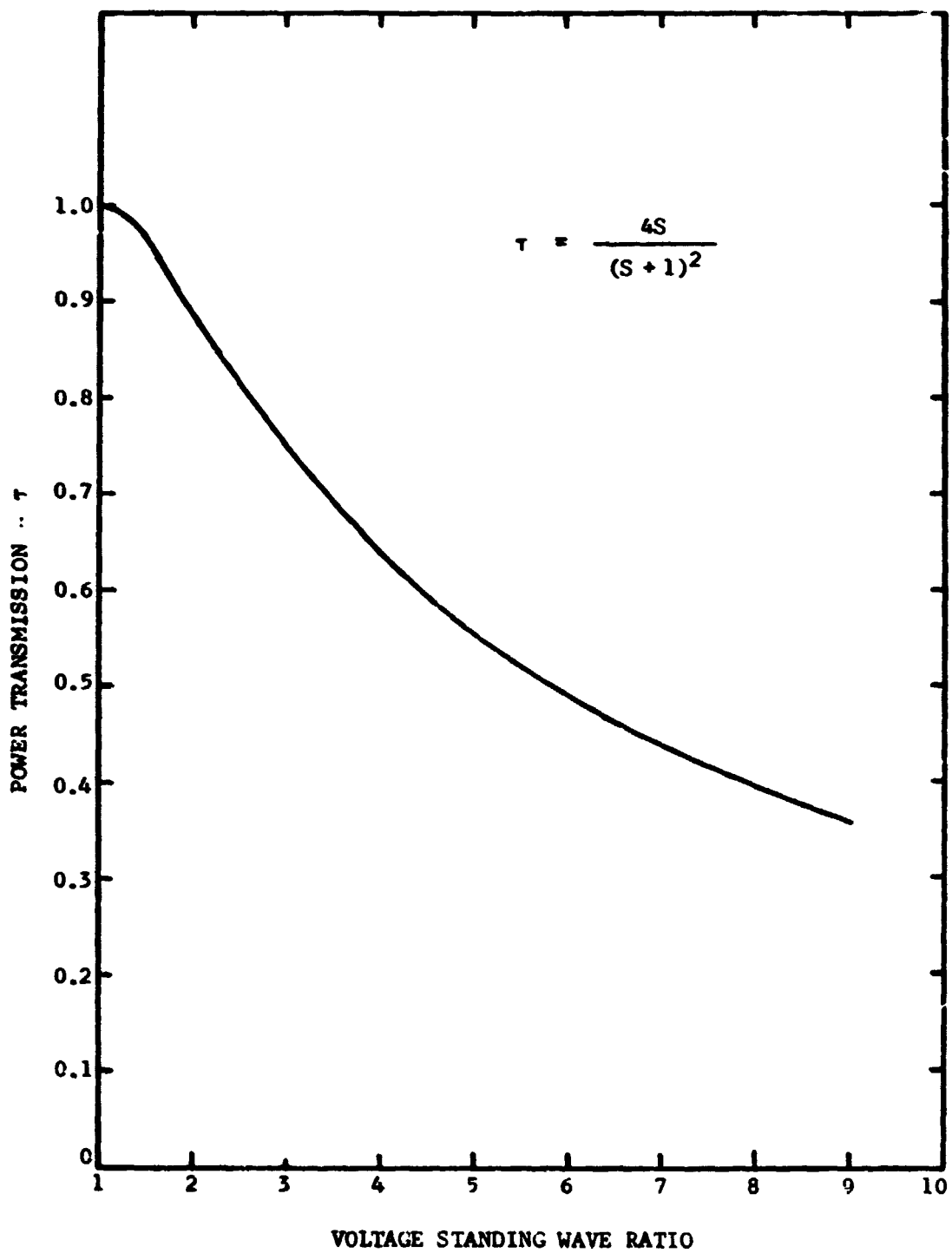


Figure 5-3 - Power Transmission versus Voltage Standing Wave Ratio

By measuring  $T_A$ ,  $T_R$  and  $S$ ,  $T_e$  can be found.  $S$  was measured to be 2.0. At 6:04 pm, when the temperature spread throughout the phantom was the greatest,  $T_e$  equalled 30.3°C.  $T_e$  is a weighted average of the temperatures throughout the layered medium, with the weighting depending on the power penetration depth. The temperature 30.3°C corresponds roughly to the temperature at a depth of 3.8 cm. Thus, it can be stated with some confidence that the radiometer sensed temperatures to a depth of, at least, 3.8 cm and, possibly, down to a depth of 5.1 cm.

### 5.3 MEASUREMENTS ON LARGE DOG

Radiometer measurements were performed at the New England Medical Center Hospital, on a Labrador male mongrel, weighing 57 lbs., with Dr. Harry H. Miller in attendance. The dog was anesthetized with pentobarbital and the left rear thigh was closely shaved. Temperature probes were positioned on the thigh surface, subcutaneous, and at depths of 1.3 and 2.5 cm. The dog and radiometer were placed in the X-ray room, to avoid interference generated by the fluorescent lights in the Surgical Research Laboratory. Other external interference was fairly slight. A 10-second time constant was used in measuring apparent temperatures, and 100 samples were taken at a rate of 1 sample/sec., for each measurement.

The measured radiometer apparent temperature and the temperatures of the surface, subcutaneous, and 1.3 cm-deep probes are plotted in Figure 5-4. Figure 5-5 shows the measured radiometer apparent temperature and the 2.5 cm deep probe plotted on an exaggerated vertical scale. The vertical bars, in Figure 5-5, indicate the measured radiometer sensitivity,  $\Delta T_A$ . As indicated by the annotations on the figures, the procedure followed consisted of the following steps:

1. Reference radiometer and temperature probe measurements were initially taken.
2. The radiometer was removed at 2:00 pm and repositioned and more reference measurements were made. This allowed for checking on how sensitive the measurements were to repositioning. The apparent temperature curve indicates that the repositioning did not have a significant effect on the measurements.

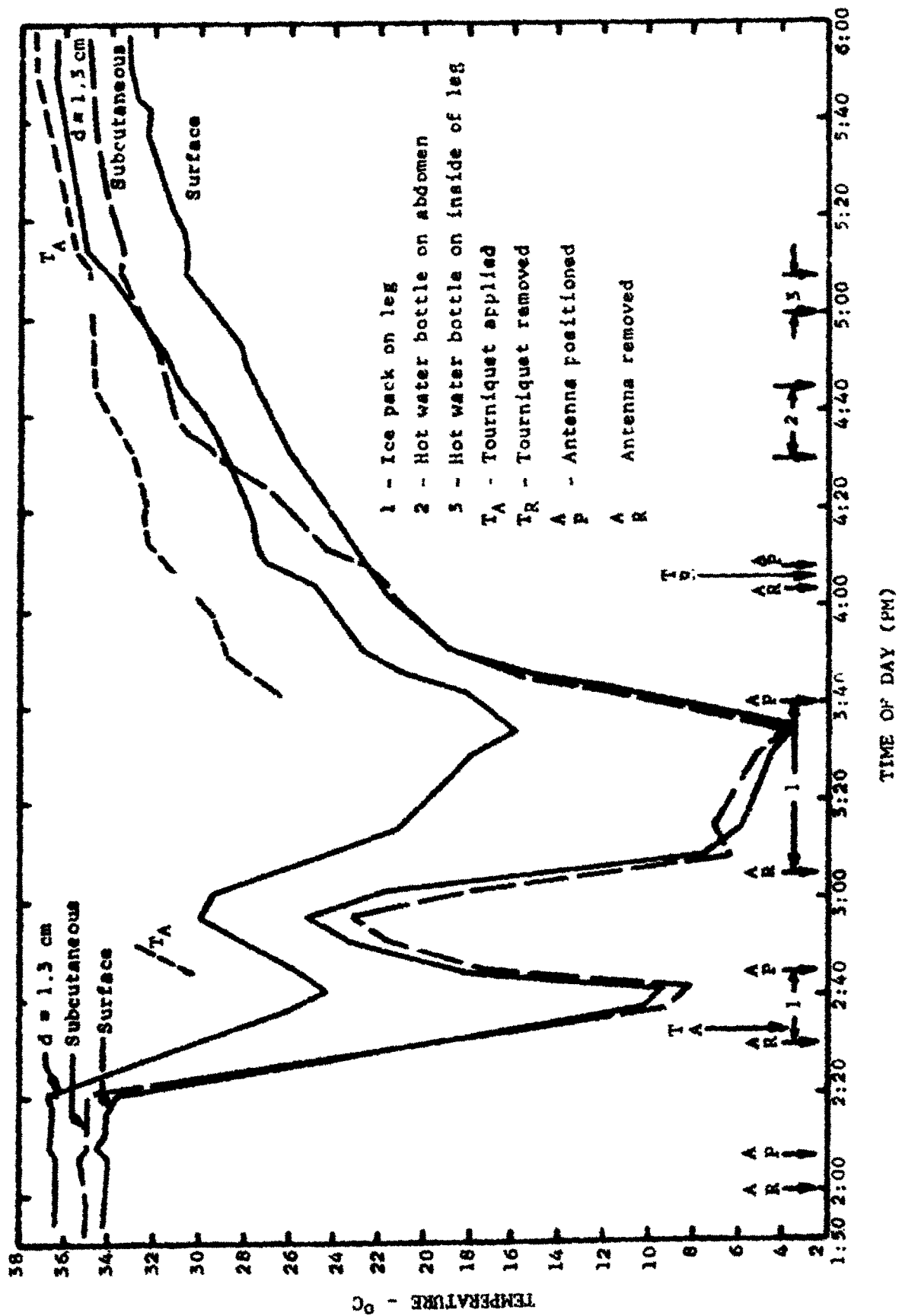


Figure 5-4 - Apparent Temperature and Temperature Data on Dog's Thigh



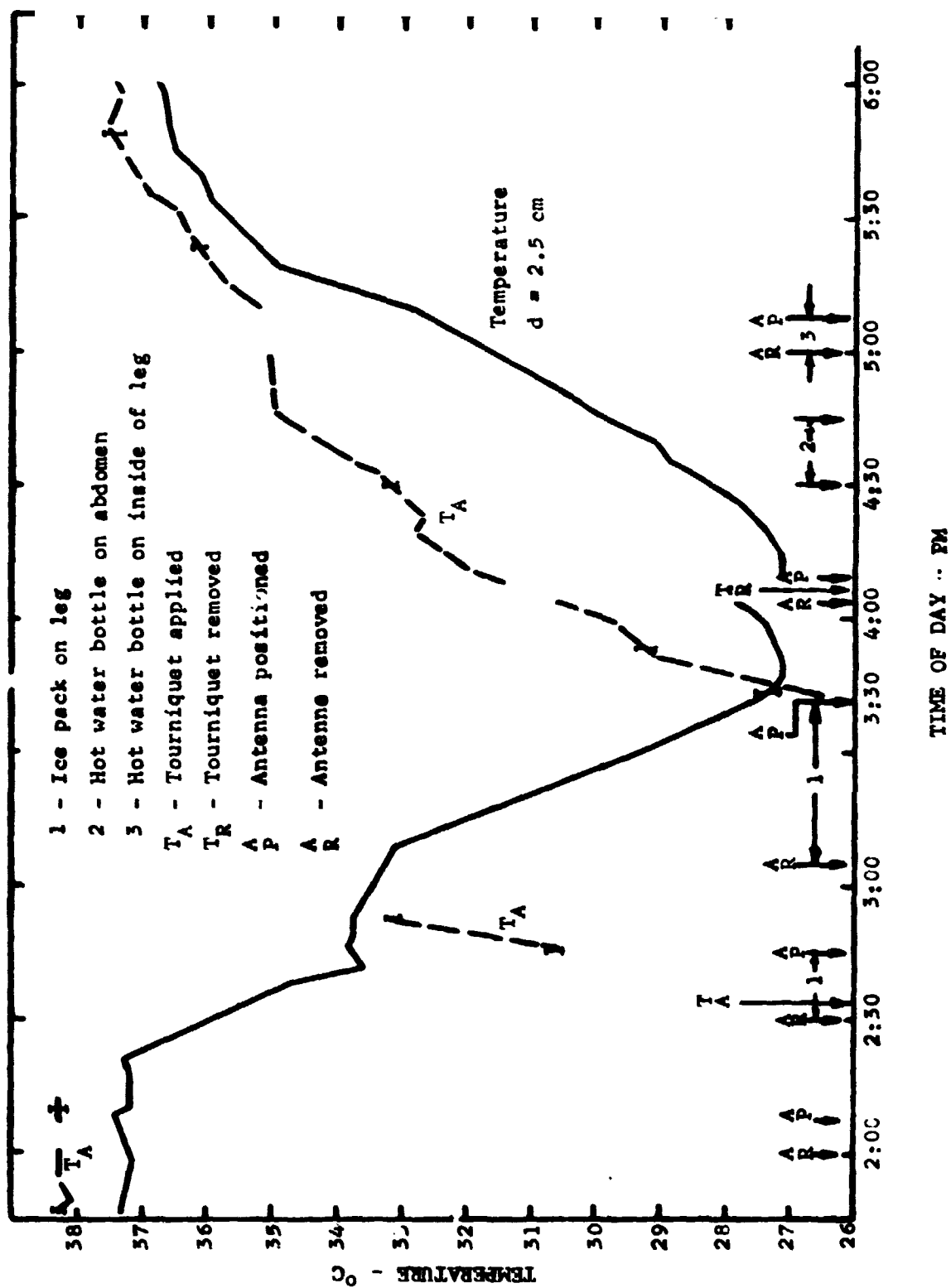


Figure 5-5 - Apparent Temperature and Temperature Data on Dog's Thigh

3. The radiometer was removed at 2:30 pm and a tourniquet and ice pack, containing an ice-alcohol mixture, was applied to the upper portion of the thigh. After the leg was cooled down, the ice pack was removed, the radiometer was repositioned, and measurements were repeated. As expected, the apparent temperature showed a sharp decrease.
4. The radiometer was removed again at 3:05 pm, and the ice pack was reapplied for further cooling. After sufficient cooling, the ice pack was removed, and the radiometer was placed back on the thigh. Measurements were taken as the thigh warmed up, during which the apparent temperature showed a steady increase.
5. At 4:05 pm the radiometer was removed so that the tourniquet could be released. The radiometer was then repositioned and the apparent temperatures continued to increase.
6. To aid in warming the leg, a hot water bottle was placed on the abdomen between 4:30 and 4:45 pm.
7. At 5:00 pm the radiometer was removed, the hot water bottle was placed on the inside of the leg for several minutes and then removed, and the radiometer was repositioned.

Referring to Figure 5-4, it will be noted that the apparent temperature curve follows the 1.3 cm-deep temperature curve fairly closely. In Figure 5-5, the correspondence between  $T_A$  and the 2.5 cm temperature curve is rather poor when the temperature is increasing except, perhaps, after 5:00 pm. Thus, on the increasing temperature portion, the apparent temperatures appear to follow temperatures at shallower depths, as indicated in Figure 5-4. It will be recalled that the penetration depth in the phantom model was somewhat greater - between 3.8 and 5.1 cm. This is probably due to the lack of circulating blood in the phantom. However, the above results are quite encouraging and it appears that indirect blood flow measurement, with a microwave radiometer, holds considerable promise.

## Section 6

### CONCLUSIONS

Several conclusions of importance may be drawn from the results of this study. These are as follows:

1. The development of a highly sensitive microwave radiometer, for use in near-field measurements of radiation from biological materials, has been successfully accomplished. Such observations are now quite practical and can be made with a high level of absolute accuracy.
2. Measurements made on a phantom model indicate that the radiometer is sensitive to temperature changes occurring in the top 0.5 cm layer of fat and, at least, the first 3.2 cm of lean beef. It is likely that temperatures as deep as 5.1 cm influenced the radiometer response. The ability of the radiometer to sense temperature changes, from these depths, establishes the feasibility of measuring subsurface temperature changes in biological tissue.
3. The close agreement between the phantom measurements and the corresponding theoretical apparent temperatures, substantiates the validity of using a layered tissue model, of infinite lateral extent, for predicting brightness temperatures in real tissue structures.
4. Measurements performed on a hind thigh of a dog indicate that the radiometer sensed temperature changes from a depth of, at least, 1.3 cm.

## Section 7

### RECOMMENDATIONS

The results of this study indicate several areas in need of further investigation, to properly develop the microwave radiometric blood flow sensing technique. These areas are presented below.

#### 7.1 INTEGRAL VSWR MEASUREMENT CIRCUIT

A VSWR measurement circuit should be designed and fabricated to mount inside the radiometer RF head. This will permit convenient and rapid measurement of VSWR, via the radiometer antenna, during future observations on phantom tissue models, dogs and human subjects. The use of bulky, standard laboratory equipment, for this purpose, is awkward and time consuming. It also requires de-mounting the antenna from the RF head. The recommended integral circuit would eliminate these problems and provide VSWR information easily and accurately.

#### 7.2 MEASUREMENT OF BLOOD DISTRIBUTION IN THE BODY

Due to problems caused by externally generated interference, the work in this study was sufficiently delayed to preclude measurements on human subjects. Accordingly, it is recommended that an extensive investigation be performed on humans to develop a technique for determining blood distribution in the body. The radiometer could be employed in measuring apparent temperatures of the head and other parts of the body, under stresses imposed by heat and exercise. Of particular interest are heat losses from various parts of the body, under specified conditions. These are unknown at present.

The radiometer is capable of sensing subsurface temperatures down to a depth of about 1.5 cm. Since a significant portion of the blood volume is in this region, measurements at different points on the body should yield a good indication of blood distribution and heat flow.

### 7.3 CORRELATIVE MEASUREMENTS OF BLOOD FLOW

As discussed in Section 4, it has been difficult to obtain accurate correlative data on blood flow during temperature and radiometric measurements. Even if the square-wave electromagnetic flowmeters had performed satisfactorily, their use is limited to a single blood vessel; thus, no indication is given of the amount of collateral flow. The other disadvantage of these instruments is that a surgical operation is required to permit their use. This precludes their application in the type of investigation described in the above Paragraph.

In view of the above problems, it is recommended that correlative data on blood flow be obtained for future radiometric investigations by either a radioisotope method, an impedance plethysmograph, the ultrasonic method, a cold mass or a heat pulse (described in Section 4) whichever is most appropriate for a given experiment. If the necessary equipment, for a particular investigation, is not readily available, consideration should be given to performing the experiment at a facility that can furnish it temporarily, on a rental basis.

### 7.4 LOWER FREQUENCY RADIOMETER

The operating RF center frequency of the radiometer, delivered to NASA-Ames, is near 800 MHz. This is about 75 MHz higher than was originally intended and was caused by the need for a bandpass filter capable of eliminating certain UHF TV frequencies.

Since the depth from which the radiometer can sense temperatures appears to be limited to about 1.5 cm, it would be worthwhile furnishing an additional RF head to operate at a lower frequency and, hence, provide a means for sensing temperatures at greater depths. Figure 2-8 shows that operation in the vicinity of 500 MHz should be optimum. The tendency of the antenna aperture to increase to objectionable proportions could be eliminated by raising the dielectric constant of the loading material to a value that would compensate for the increase in aperture. It has been recently discovered that loading materials with dielectric constants above 30 are manufactured by the Raytheon Company.

Operation at a lower frequency could permit temperature measurements on organs located at some depth in the body. An ideal approach would involve a 3-frequency radiometer. Since each frequency would be limited to a particular depth, such an instrument could be designed to three temperatures simultaneously, in profile, to a depth dictated by the lowest frequency. This approach would permit a better understanding of heat flow from the body.

8. REFERENCES

1. Pennock, B., private communication, August, 1969. Dr. Pennock is with the Department of Physiology and Biophysics at Woman's Medical College of Pennsylvania, Philadelphia, PA.
2. Dicke, R.H., "The Measurement of Thermal Radiation at Microwave Frequencies", Review of Scientific Instruments, 1946, Vol. 17, p. 268.
3. Stow, Richard W., "Thermal Measurement of Tissue Blood Flow", Department of Physical Medicine, the Ohio State University, Columbus, Ohio. Published in Transactions of the New York Academy of Sciences, April 1965.

**APPENDIX A**

**LISTINGS OF COMPUTER PROGRAMS**

**SETUP 1**

**SETUP 2**

**RADIOM**

**PBTEMP**

**RADRMS**



```

DIMENSION A(130),H(500),ATEST(4) SET00010
DATA ATEST/1< 1,1> 1,1= 1,1? 1/ SET00020
DATA ATESTX/11 1/ SET00030
DATA ATEST0/10 1/ SET00040
DATA ATEST2/12 1/ SET00050
DATA ATEST3/13 1/ SET00060
DATA ATEST9/19 1/ SET00070
READ(1,1000) A SET00080
1000 FORMAT(130A1) SET00090
1 CONTINUE SET00100
IREG=1 SET00110
IEND=130 SET00120
IF(A(3).EQ.ATEST9.AND.A(4).EQ.ATEST9) GO TO 999 SET00130
10 CONTINUE SET00140
J=0 SET00150
DO 20 I=IREG,IEND SET00160
J=J+1 SET00170
IF(A(J).EQ.ATESTX) GO TO 30 SET00180
IF(I.GT.500) GO TO 40 SET00190
ISAVE=I SET00200
H(I)=A(J) SET00210
20 CONTINUE SET00220
30 CONTINUE SET00230
READ(1,1000) A SET00240
IF(A(11).EQ.ATEST(4).AND.A(12).EQ.ATEST(4).AND.A(13).EQ.ATEST(4) SET00250
X.AND.A(14).EQ.ATEST(4)) GO TO 50 SET00260
IREG=ISAVE+1 SET00270
IEND=IREG+129 SET00280
GO TO 10 SET00290
40 CONTINUE SET00300
WRITE(5,5000) SET00310
5000 FORMAT(23H DATA IN INCORRECT FORM) SET00320
CALL EXIT SET00330
50 CONTINUE SET00340
ISTOP=ISAVE SET00350
IREG=1 SET00360
IEND=14 SET00370
WRITE(2,2000) (H(I),I=IREG,IEND) SET00380
2000 FORMAT(14A1) SET00390
IF(H(5).EQ.ATEST(3).OR.H(5).EQ.ATEST(4)) GO TO 80 SET00400
DO 60 I=15,78 SET00410
ISAVE=I SET00420
IF(H(I).EQ.ATEST0.AND.H(I+1).EQ.ATEST0.AND.H(I+2).EQ.ATEST0 SET00430
X.AND.H(I+4).EQ.ATEST2.AND.H(I+5).EQ.ATEST3.AND.H(I+8) SET00440
X.EQ.ATEST4.AND.H(I+9).EQ.ATEST9.AND.H(I+10).EQ.ATEST9) SET00450
XGO TO 70 SET00460
60 CONTINUE SET00470
WRITE(2,2001) ATEST9,ATEST4,ATEST4,ATEST9 SET00480
2001 FORMAT(4A1) SET00490
GO TO 1 SET00500
70 CONTINUE SET00510
IREG=ISAVE-52 SET00520
IEND=ISAVE+11 SET00530
WRITE(2,2002) (H(I),I=IREG,IEND) SET00540
2002 FORMAT(64A1) SET00550

```

NO CONTINUE	SET00560
IREG=IEND+1	SET00570
IEND=ISTOP	SET00580
NUMRAD=(IEND-IREG+1)/4	SET00590
IREG=(IEND-4*NUMRAD)+1	SET00600
WRITE(2,2003) NUMRAD	SET00610
2003 FORMAT(I3)	SET00620
WRITE(2,2002) (H(I),I=IREG,IEND)	SET00630
GO TO 1	SET00640
999 CONTINUE	SET00650
WRITE(2,2001) ATEST9,ATEST9,ATEST9,ATEST9	SET00660
CALL EXIT	SET00670
END	SET00680

DIMENSION R(500),A(10)	SET00010
DATA AX/'=    '/	SET00020
DATA AY/'?    '/	SET00030
DATA A/'1    1.12    1.13    1.14    1.15    1.	SET00040
X'6    1.17    1.18    1.19    1.20    '/	SET00050
1 CONTINUE	SET00060
READ(1,1000) (H(I),I=1,14)	SET00070
WRITE(2,1000) (H(I),I=1,14)	SET00080
1000 FORMAT(14A1)	SET00090
IF(H(3).EQ.A(9).AND.H(4).EQ.A(9)) CALL EXIT	SET00100
IF(R(5).EQ.AX.OR.H(5).EQ.AY) GO TO 35	SET00110
READ(1,1001) (H(I),I=1,64)	SET00120
1001 FORMAT(64A1)	SET00130
IF(R(1).EQ.A(9).AND.H(2).EQ.A(9).AND.H(3).EQ.A(9)	SET00140
X.AND.H(4).EQ.A(9)) GO TO 999	SET00150
DO 30 I=1,64	SET00160
DO 10 J=1,10	SET00170
IF(R(I).EQ.A(J)) GO TO 30	SET00180
10 CONTINUE	SET00190
KREG=((I-1)/4)*4+1	SET00200
KEND=KREG+3	SET00210
DO 20 K=KREG,KEND	SET00220
20 B(K)=A(R)	SET00230
30 CONTINUE	SET00240
WRITE(2,1001) (H(I),I=1,64)	SET00250
35 CONTINUE	SET00260
READ(1,1002) NUMRAD	SET00270
1002 FORMAT(I3)	SET00280
IEND=NUMRAD*4	SET00290
READ(1,1001) (H(I),I=1,IEND)	SET00300
IF(NUMRAD.LT.3) GO TO 80	SET00310
NCOUNT=0	SET00320
DO 60 I=5,IEND	SET00330
DO 50 J=1,10	SET00340
IF(R(I).EQ.A(J)) GO TO 60	SET00350
50 CONTINUE	SET00360
NCOUNT=NCOUNT+1	SET00370
IF(NCOUNT.EQ.2) GO TO 998	SET00390
K=4	SET00390
IF(IEND-I.LT.4) K=-4	SET00400
R(I)=R(I+K)	SET00410
60 CONTINUE	SET00420
GO TO 100	SET00430
80 R(5)=A(10)	SET00440
R(6)=A(10)	SET00450
R(7)=A(10)	SET00460
R(8)=A(10)	SET00470
100 CONTINUE	SET00480
R(1)=R(5)	SET00490
R(2)=R(6)	SET00500
R(3)=R(7)	SET00510
R(4)=R(8)	SET00520
WRITE(2,1002) NUMRAD	SET00530
WRITE(2,1001) (H(I),I=1,IEND)	SET00540
GO TO 1	SET00550

```
998 NUMRAD=999  
  WRITE(2,1002) NUMRAD  
  GO TO 1  
999 WRITE(2,1001) (H(I),I=1,64)  
  GO TO 1  
END
```

```
SET00560  
SET00570  
SET00580  
SET00590  
SET00600  
SET00610
```

```

    DIMENSION TITLE(10,13)
    DIMENSION ATEST(8)
    DIMENSION IVOLT(100),TFMPR(13)
    DIMENSION CALR(2),ITIME(4)
    DATA ATEST/1< 0.1> 0.1= 0.1? 0.1> 0.1= 0,
X18 0.07 0/
    ITIME(1)=0
    ITIME(2)=0
    ITIME(3)=0
    ITIME(4)=0
    CALR(1)=0.
    CALR(2)=1.
    KCT=0
    READ(5,5000) TITLE
5000 FORMAT(10A4)
    ) CONTINUE
    WRITE(9,9000)
    WRITE(6,6000)
6000 FORMAT(2H X)
9000 FORMAT(1H1////////24X,24H* * * RDS READ OUT * * *//)
    READ(2,2000) NSAMPL,NEXP,STATUS,RATE,NX1,NX2,NY1,NY2,D
2000 FORMAT(2I2,2A1,4I1,A4)
    IF(NEXP.EQ.99) CALL EXIT
    IF(NSAMPL.EQ.0) NSAMPL=100
    WRITE(9,9001) NEXP,NX1,NX2,NY1,NY2
9001 FORMAT(11X,20H EXPERIMENT NUMBER = ,I2/
X11X,7H TIME = ,2I1,1H: ,2I1/)
    IF(STATUS.EQ.ATEST(1).OR.STATUS.EQ.ATEST(3)) WRITE(9,9002)
    IF(STATUS.EQ.ATEST(2).OR.STATUS.EQ.ATEST(4)) WRITE(9,9003)
    IF(STATUS.EQ.ATEST(3).OR.STATUS.EQ.ATEST(4)) WRITE(9,9004)
    IF(STATUS.EQ.ATEST(1).OR.STATUS.EQ.ATEST(2)) WRITE(9,9005)
9002 FORMAT(10X,27H RADIOMETER IN OPERATE MODE)
9003 FORMAT(10X,29H RADIOMETER IN CALIBRATE MODE)
9004 FORMAT(10X,26H TEMPERATURES NOT RECORDED/)
9005 FORMAT(10X,22H TEMPERATURES RECORDED/)
    IF(RATE.EQ.ATEST(5)) IRATE=1
    IF(RATE.EQ.ATEST(6)) IRATE=2
    IF(RATE.EQ.ATEST(7)) IRATE=4
    IF(RATE.EQ.ATEST(8)) IRATE=5
    WRITE(9,9006) IRATE,NSAMPL
9006 FORMAT(10X,15H SAMPLE RATE = ,I1,4H/SEC/
X10X,31H NUMBER OF RADIOMETER SAMPLES = ,I3//)
    IF(STATUS.EQ.ATEST(3).OR.STATUS.EQ.ATEST(4)) GO TO 30
    READ(2,2001) (IVOLT(I),I=1,16)
2001 FORMAT(16I4)
    IF(IVOLT(1).NE.9999) GO TO 10
    WRITE(9,9007)
9007 FORMAT(////10X,36H CALIBRATION SEQUENCE WAS NOT FOUND.)
    KCT=0
    GO TO 1
    10 CONTINUE
    WRITE(9,9008) (IVOLT(I),I=14,16)
9008 FORMAT(22X,15HRDS CALIBRATION/11X,
X35HZERO    PROBE SCALE    FULL SCALE/
X11X,I3,9X,I4,12X,I4//)

```

```

      IF (IVOLT(15).EQ.0) IVOLT(15)=1
      DO 20 I=1,13
      RES=IVOLT(I)*9451./IVOLT(15)
      OFFSET=0.
      IF (I.EQ.1) OFFSET=-.3
      CALL PTEMP(RES,OFFSET,TEMPR(I))
      IF (TEMPR(I).LT.0.) TEMPR(I)=WFS*.1
20 CONTINUE
      WRITE(9,9009) ((TITLE(I,J)*I=1,10),TEMPR(J),J=1,13)
9009 FOR 'AT(24X,27H PROBE TEMPERATURES (DEG C))//
      X.10X,6H R1 = .10A4,3H = .F6,1,2H C/
      X.10X,6H R2 = .10A4,3H = .F6,1,2H C/
      X.10X,6H R3 = .10A4,3H = .F6,1,2H C/
      X.10X,6H R4 = .10A4,3H = .F6,1,2H C/
      X.10X,6H R5 = .10A4,3H = .F6,1,2H C/
      X.10X,6H R6 = .10A4,3H = .F6,1,2H C/
      X.10X,5H R7 = .10A4,3H = .F6,1,2H C/
      X.10X,6H R8 = .10A4,3H = .F6,1,2H C/
      X.10X,6H R9 = .10A4,3H = .F6,1,2H C/
      X.10X,7H R10 = .10A4,3H = .F6,1,2H C/
      X.10X,7H R11 = .10A4,3H = .F6,1,2H C/
      X.10X,7H R12 = .10A4,3H = .F6,1,2H C/
      X.10X,7H R13 = .10A4,3H = .F6,1,2H C)
      WRITE(3,3000) NX1,NX2,NY1,NY2,TEMPR
3000 FORMAT(4I1,13F5,1)
30 CONTINUE
      READ(2,2002) NUMRAD
2002 FORMAT(I3)
      IF (NUMRAD.EQ.999) GO TO 39
      READ(2,2001) (IVOLT(I),I=1,NUMRAD)
      IF (NUMRAD.EQ.NSAMPL) GO TO 40
39 CONTINUE
      WRITE(9,9010)
9010 FORMAT(///10X,24HEXOR IN RADIOMETER DATA)
      KCT=0
      GO TO 1
40 CONTINUE
      CALL RADRMS(IVOLT,NUMRAD,XMEAN,RMS,CHI)
      WRITE(9,9011) XMEAN,RMS,CHI
9011 FORMAT(///10X,25HMEAN RADIOMETER OUTPUT = .F6,1/
      X10X,16HRMS DEVIATION = .F6,1/
      X10X,18HCHI-SQUARE TEST = .E10,3)
      ICAL=0
      IF (STATUS.FQ.ATEST(2).OR.STATUS.EQ.ATEST(4)) ICAL=1
      WRITE(4,4000) NX1,NX2,NY1,NY2,ICAL,XMEAN,RMS,CHI
4000 FORMAT(5I1,2F7,2,E10,3)
      KCT=KCT+1
      IF (ICAL.EQ.1) GO TO 100
      KCT=0
      DENOM=CALR(2)-CALH(1)
      IF (DENOM.LT..000001) DENOM=.000001
      ATEMP=53.05*(XMEAN-CALH(1))/DENOM+TEMPR(2)+273.2
      RMSATP=53.05*RMS/DENOM
      WRITE(9,9012) ATEMP,RMSATP,ITIME
9012 FORMAT(///10X,21HAPARENT TEMPERATURE =.F7,2,6H DEG K/

```

RAD00560  
 RAD00570  
 RAD00580  
 RAD00590  
 RAD00600  
 RAD00610  
 RAD00620  
 RAD00630  
 RAD00640  
 RAD00650  
 RAD00660  
 RAD00670  
 RAD00680  
 RAD00690  
 RAD00700  
 RAD00710  
 RAD00720  
 RAD00730  
 RAD00740  
 RAD00750  
 RAD00760  
 RAD00770  
 RAD00780  
 RAD00790  
 RAD00800  
 RAD00810  
 RAD00820  
 RAD00830  
 RAD00840  
 RAD00850  
 RAD00860  
 RAD00870  
 RAD00880  
 RAD00890  
 RAD00900  
 RAD00910  
 RAD00920  
 RAD00930  
 RAD00940  
 RAD00950  
 RAD00960  
 RAD00970  
 RAD00980  
 RAD00990  
 RAD01000  
 RAD01010  
 RAD01020  
 RAD01030  
 RAD01040  
 RAD01050  
 RAD01060  
 RAD01070  
 RAD01080  
 RAD01090  
 RAD01100

X10X.11HRMS NOISE =.F7.2.6M DEG K/	RAD01110
X10X.31HBASED ON CALIBRATION AT TIME = .211.1M:.211)	RAD01120
GO TO 1	RAD01130
100 CONTINUE	RAD01140
IF (KCT.F0.1) GO TO 110	RAD01150
CALR(1)=CALSAV	RAD01160
CALR(2)=XMEAN	RAD01170
ITIME(1)=NX1	RAD01180
ITIME(2)=NX2	RAD01190
ITIME(3)=NY1	RAD01200
ITIME(4)=NY2	RAD01210
KCT=0	RAD01220
GO TO 1	RAD01230
110 CALSAV=XMEAN	RAD01240
GO TO 1	RAD01250
END	RAD01260

```
SUBROUTINE PHTEMP(WFS, OFFSET, TEMP)
DIMENSION ACOF(6), HCOF(6), CCOF(6)
DATA ACOF/0.12278E-05, 0.20540E-05, 0.32396E-05,
X0.48228E-05, 0.78230E-05, 0.11567E-04/
DATA HCOF/-0.14687E-01, -0.14336E-01, -0.24584E-01,
X-0.30371E-01, -0.34312E-01, -0.48434E-01/
DATA CCOF/51.603, 54.110, 63.445, 69.239, 75.904, 81.465/
ICOF=6
IF (RES.LT.984.2) GO TO 10
IF (RES.GT.3539) GO TO 10
IF (RES.GT.1200) ICOF=5
IF (RES.GT.1471) ICOF=4
IF (RES.GT.1815) ICOF=3
IF (RES.GT.2253) ICOF=2
IF (RES.GT.2814) ICOF=1
TFMP=ACOF(ICOF)*WFS*WFS+HCOF(ICOF)*RES+CCOF(ICOF)*OFFSET
RETURN
10 TFMP=-1.
RETURN
END
```

PBT00010  
PBT00020  
PBT00030  
PBT00040  
PBT00050  
PBT00060  
PBT00070  
PBT00080  
PBT00090  
PBT00100  
PBT00110  
PBT00120  
PBT00130  
PBT00140  
PBT00150  
PBT00160  
PBT00170  
PBT00180  
PBT00190  
PBT00200



```

SURROUTINE RADRMS(KIN,N,XMEAN,XRMS,CHI)
DIMENSION KIN(100)
TOTAL=0.
DO 10 I=1,N
TOTAL=TOTAL+KIN(I)
10 CONTINUE
XMEAN=TOTAL/N
TOTAL=0.
DO 20 J=1,N
TOTAL=TOTAL+(XMEAN-KIN(I))**2
20 CONTINUE
XMS=TOTAL/(N-1)
J=0
TOTAL=0.
DO 30 I=1,N
DEV=(XMEAN-KIN(I))**2
IF(DEV.GT.9.*XMS) GO TO 30
J=J+1
KIN(J)=KIN(I)
TOTAL=TOTAL+KIN(J)
30 CONTINUE
XMEAN=TOTAL/J
TOTAL=0.
DO 40 I=1,J
TOTAL=TOTAL+(XMEAN-KIN(I))**2
40 CONTINUE
XRMS=SQRT(TOTAL/(J-1))
L1=0
L2=0
L3=0
L4=0
DO 50 I=1,J
IF(KIN(I).GT.(XMEAN+XRMS/2.)) GO TO 41
IF(KIN(I).GT.XMEAN) GO TO 42
IF(KIN(I).GT.(XMEAN-XRMS/2.)) GO TO 43
L1=L1+1
GO TO 50
41 L4=L4+1
GO TO 50
42 L3=L3+1
GO TO 50
43 L2=L2+1
50 CONTINUE
Q1=.3085*J
Q2=.1915*J
CHI=((L1-Q1)**2/Q1)+((L2-Q2)**2/Q2)
X+((L3-Q2)**2/Q2)+((L4-Q1)**2/Q1)
RETURN
END
RAD00010
RAD00020
RAD00030
RAD00040
RAD00050
RAD00060
RAD00070
RAD00080
RAD00090
RAD00100
RAD00110
RAD00120
RAD00130
RAD00140
RAD00150
RAD00160
RAD00170
RAD00180
RAD00190
RAD00200
RAD00210
RAD00220
RAD00230
RAD00240
RAD00250
RAD00260
RAD00270
RAD00280
RAD00290
RAD00300
RAD00310
RAD00320
RAD00330
RAD00340
RAD00350
RAD00360
RAD00370
RAD00380
RAD00390
RAD00400
RAD00410
RAD00420
RAD00430
RAD00440
RAD00450
RAD00460
RAD00470
RAD00480
RAD00490

```